Donor and acceptor substituted triphenylamines exhibiting bipolar charge-transporting and NLO properties

Dalius Gudeika, Arturs Bundulis, Igors Mihailovs, Dmytro Volyniuk, Juozas V. Grazulevicius, Martins Rutkis

Graphical Abstract

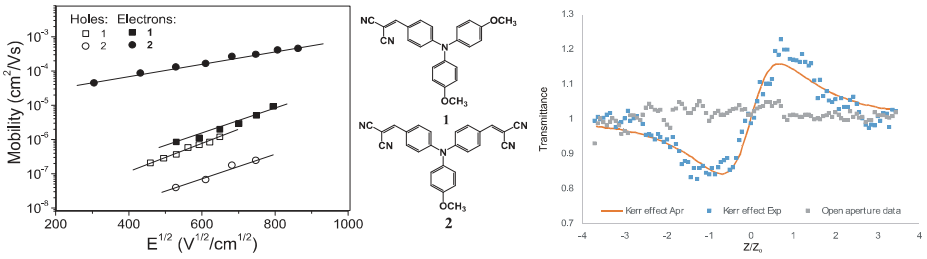

Donor and acceptor substituted triphenylamines exhibiting bipolar charge-transporting and NLO properties

Dalius Gudeika[1], Arturs Bundulis[2], Igors Mihailovs[2], Dmytro Volyniuk[1], Martins Rutkis[2], Juozas V. Grazulevicius[1]

[1] *Department of Organic Technology, Kaunas University of Technology, Radvilenu pl. 19, LT-50254, Kaunas, Lithuania*

[2] *Institute of Solid State Physics, University of Latvia, 8 Kengaraga St., Riga LV-1063, Latvia*

Corresponding author. E-mail address: juogra@ktu.lt (Juozas Vidas Gražulevičius)

Abstract

Donor-acceptor type triphenylamine-based malonodinitriles were synthesized and their thermal, optical, photophysical, electrochemical and nonlinear optical properties were studied. The synthesized compounds formed glasses with the glass transition temperatures ranging from 38 to 107 °C. The ionization potentials of the samples of the compounds established by cyclic voltammetry were found to be in the range of 5.50-5.57 eV, while those estimated by photoelectron emission spectrometry ranged from 5.36 to 5.74 eV. The electron affinity values of the compounds were found to be in the range of -3.41 – -3.05 eV. The ambipolar charge-transporting properties were observed for the layers of triphenylamine-based malonodinitriles. Hole mobilities of the layers of the compounds were in the range of 10^{-7} - 10^{-6} $cm^2/V \cdot s$, while electron mobilities were by *ca.* two orders of magnitude higher. All the synthesized compounds had positive sign for second order hyperpolarizability.

Keywords: triphenylamine, malonodinitrile, glass transition temperature, ambipolar, second order hyperpolarizability.

1. INTRODUCTION

Low-molar-mass amorphous molecular materials having intramolecular charge transfer (ICT) properties represent an interesting class of materials which attracts increasing attention [1,2]. Such materials usually contain both electron-accepting and electron-donating moieties [3,4]. Compared to polymeric compounds, where batch to batch synthetic reproducibility, purification and product characterization are often rather difficult tasks, the molecular materials are much easier to obtain, isolate, identify and purify [5]. Organic materials having triphenylamino moiety have attracted attention of both experimental and theoretical communities due to their useful thermal, electrochemical, photoelectrical and photophysical properties [6-8]. Triphenylamine (TPA) and its derivatives, with excellent solubility, good stability, and high photoluminescent efficiency, have been extensively used in optoelectronic and electronic devices [9], such as organic light emitting diodes (OLEDs) [10,11], dye-sensitized solar cells [12], field-effect transistors [13]. The electron-donating nature of TPA moiety predetermines good hole-transporting properties and low ionization potentials of the layers of the TPA derivatives [14]. Owing to the noncoplanarity of the three phenyl rings, TPA derivatives can be viewed as 3D systems [15]. In this context much effort has been made to understand the relationship between their molecular structure and the charge-transporting properties [16,17]. Generally, using TPA derivatives it is possible to obtain compounds which demonstrate reversible oxidation and high electrochemical stability [18].

The last decade has witnessed a notable increase of attention in organic materials with nonlinear optical (NLO) properties [19], making these compounds viable for practical applications in various photonic devices [20]. In the case of NLO materials where the active part of the material is a push-pull type chromophore with high molecular hyperpolarizability (β) values, the formation of a stable solid amorphous phase is rather hard task [21]. The chromophores used in such materials are usually linear,

planar and polar moieties which contradict with the general structural requirements of a good glass-formation. Organic materials exhibiting both photoconducive and NLO properties are of interest for the application as photorefreactive materials. The applications of organic photorefractive materials include biomedical imaging, optical computing, image and signal processing, holographic filters, 3D display technology [22].

It is known that cyano group is one of the strongest electron-withdrawing groups [23]. Electron-accepting effect can be enhanced by introducing several cyano moieties into a π-electronic system [24]. Compounds having triphenylamino and dicyanovinyl moieties were synthesized and investigated as solvatochromic fluorescent dyes [25]. However, to our knowledge, no studies on the sructure-properties relationship of the derivatives of TPA containing dicyanovinyl moieties and the different number of methoxy and methyl groups were yet reported. The role of the methoxy groups was found to be related to the mesomeric effect and the possibility to establish hydrogen bonds [26]. The possibility to monitor ionization potentials of TPA derivatives by attaching different donor and/or acceptor moieties is also important in the design and fabrication of OLEDs and other optoelectronic devices.

With the aim to explore the relationship between chemical structures and various properties of bipolar compounds we performed the simple synthesis of TPA derivatives containing both electron-donating methyl and/or methoxy groups and accepting dicyanovinyl moieties and studied their thermal, photophysical, electrochemical, charge-transporting and non-linear optical properties.

2. EXPERIMENTAL

2.1. Materials and instrumentation

Triphenylamine (**TPA**), malonodinitrile, zinc acetate dihydrate ($Zn(CH_3COO)_2 \cdot 2H_2O$) were purchased from Aldrich and used without further purification.

^1H and ^{13}C NMR spectra were recorded using Bruker Avance III (700 MHz (^1H), 176 MHz (^{13}C)) spectrometer at room temperature. Infrared (IR) spectra were taken using Perkin Elmer Spectrum GX spectrometer. Mass (MS) spectra were obtained on a Waters ZQ 2000 (Milford, USA). Elemental analysis was performed with an Exeter Analytical CE-440 Elemental Analyser. Differential scanning calorimetry (DSC) measurements were carried out using a Q100 TA DSC series thermal analyzer at a heating rate of 10 ^oC/min under nitrogen flow. Thermogravimetric analysis (TGA) measurements were performed on a Mettler Toledo TGA/SDTA 851^e under nitrogen. Melting points (m.p.) were recorded on Electrothermal Mel-Temp melting point apparatus. UV absorption spectra were recorded on Perkin Elmer Lambda 35 spectrometer. Fluorescence (FL) spectra of dilute solutions and of neat films were recorded by FLS980 fluorescence spectrometer with TMS300 monochromators and a red cooled detector (Hamamatsu R928P). The standard light source for measuring of FL spectra was a 450 W xenon arc lamp. Fluorescence quantum yields (Φ_F) of the solutions and solid films were carried out by absolute method using integrated sphere of 120 mm inside diametre of the spherical cavity. The measurements were carried out at the room temperature. The cyclic voltammetry (CV) measurements were carried out by a three-electrode assembly cell from Bio-Logic SAS and a micro-AUTOLAB Type III potentiostat-galvanostat. The working electrode was a glassy carbon, the reference electrode and the counter electrode were Ag/Ag^+ 0.01 M and Pt wire, respectively. Argon-purged dichloromethane with tetrabulthylammonium hexafluorophosphate (Bu_4NPF_6) 0.1 M was used as electrolyte. The experiments were calibrated with the standard ferrocene/ferrocenium redox system [27]. Half-wave redox potential for Fc/Fc^+ was established to be 0.295 V *vs.* Ag. Solid-state ionization potentials (IP_{EP}) were established by electron photoemission in air method [28,29]. For the measurements the layers on ITO glass were prepared by drop casting from the solutions of the compounds in tetrahydrofuran (THF). The samples were illuminated with the monochromatic light obtained using the deep UV deuterium light source ASBN-D130-CM and CM110 1/8 m

monochromator. The negative voltage of 500 V was supplied to the sample substrate. The counter-electrode was placed at the distance of 3 mm from the sample surface. The counter-electrode was connected to the input of the 6517B Keithley electrometer for the photocurrent measurement. An energy scan of the incident photons was performed while increasing the photon energy *hv*. In this scan direction, no electrons were emitted until *hv* exceeded the ionization potential of the layer. Charge transporting porperties were investigated by the time of light (TOF) measurements as reported earlier [30,31]. A third harmonic of pulsed Nd:YAG laser (EKSPLA NL300, a wavelength of 355 nm, pulse duration 3-6 ns) was used for photoexcitation. The photocurrent transients at different electric fields were measured across a load resistor by the Tektronix TDS 3052C oscilloscope. The transit time (t_{tr}) was determined at time where a change of the slope in the photocurrent transients was observed. The carrier mobility μ was calculate by the relation $\mu = d^2/Vt_{tr}$, where d is the thickness of the studied films and V is the applied voltage to the electrodes of the TOF structures. To analyze Kerr effect and two photon absorption z-scan method was used. Experimental setup is shown in Fig. S1. In this method the sample is moved parallel to a focused laser beam through the focal point. The information on two-photon absorption and Kerr effect was acquired by analyzing normalized transmission as a function of sample position. For two-photon absorption total laser power as function of sample position (open aperture) was measured. For Kerr effect laser irradiance as function of sample position (closed aperture) was measured. To do this, a small (in comparison with beam size) aperture (diameter d = 1 mm) was placed before detector. For Kerr effect, the refractive index can be written as: $n = n_0 + n_2 \cdot I_0$, where n_0 is linear refractive index, n_2 is nonlinear refractive index and I_0 is the optical intensity. In case of two-photon absorption: $\alpha = \alpha_0 + \alpha_2 \cdot I_0$, where α is materials absorption, α_0 is linear absorption coefficient and α_2 is nonlinear absorption coefficient. For z-scan setup a 1064 nm Nd:YAG laser with 30 ps-duration at a 10 Hz repetition rate was used.

2.2. Synthesis

4-Methoxy-*N*-(4-methoxyphenyl)-*N*-phenylaniline (**a**, m.p. = 104-105 °C, lit. [32] m.p. = 103 °C), 4-diphenylaminoanisole (**b**, m.p. = 99-100 °C, lit. [33] m.p. = 102 °C), di(*p*-tolyl)(*p*-methoxyphenyl)amine (**c**, m.p. = 71-72 °C, lit. [34] m.p. = 70-73 °C), 4-diphenylaminotoluene (**d**, m.p. = 68-70 °C, lit. [33] m.p. = 68.8 °C), 4-[bis(4-methoxyphenyl)amino]benzaldehyde (**e**, m.p. = 91-93 °C, lit. [35] m.p. = 92-93 °C), 4-[(4-formylphenyl)(4-methoxyphenyl)amino]benzaldehyde (**f**, m.p. = 82-84 °C, lit. [35] m.p. = 83-84 °C), 4-[bis(4-methylphenyl)amino]benzaldehyde (**g**, m.p. = 98-99 °C, lit. [35] m.p. = 97-98 °C) and 4-[(4-formylphenyl)(4-methylphenyl)amino]benzaldehyde (**h**, m.p. = 143-144 °C, lit. [35] m.p. = 142-143 °C), were synthesized by the earlier described procedures.

2-(4-(Bis(4-methoxyphenyl)amino)benzylidene)malononitrile (1). To a solution of 4-[bis(4-methoxyphenyl)amino]benzaldehyde (**e**) (0.80 g, 2.34 mmol) and malonodinitrile (0.16 g, 2.34 mmol) in dehydrated *N*,*N*-dimethylformamide (15 mL), $Zn(OAc)_2 \cdot 2H_2O$ (0.53 g, 2.34 mmol) was added at room temperature. After 3 h the reaction mixture was washed with water (2×150 mL), extracted with chloroform and dried over Na_2SO_4. After removal of the solvent under the reduced pressure, the residue was purified with column chromatography (silica gel, *n*-hexane/EtOAc, 3:1, v/v). The product was recrystallized from the mixture of solvents of the eluent. The yield of orange crystals was 0.44 g, 68%. $C_{24}H_{19}N_3O_2$, MW = 381.44 g/mol, mp = 140-141 °C.

2,2'-(4,4'-(4-Methoxyphenylazanediyl)bis(4,1-phenylene)bis(methan-1-yl-1-ylidene))dimalononitrile (2) was obtained by the similar procedure as **1** using 4-[(4-formylphenyl)(4-methoxyphenyl)amino]benzaldehyde (**f**) (0.50 g, 1.51 mmol), malonodinitrile (0.20 g, 3.02 mmol), $Zn(OAc)_2 \cdot 2H_2O$ (0.53 g, 2.34 mmol). The crude product was purified with column chromatography (silica gel, *n*-hexane/EtOAc, 4:1, v/v). The product was recrystallized from the mixture of solvents of the eluent. The yield of red crystals was 0.59 g, 92%. $C_{27}H_{17}N_5O$, MW = 427.47 g/mol, mp = 150-151 °C.

2-(4-(Bis(4-methylphenyl)amino)benzylidene)malononitrile (3). Compound **3** was obtained by the similar procedure as **1** using 4-formyl-4',4''-dimethylphenylamine (**g**) (0.07 g, 0.23 mmol), malonodinitrile (0.02 g, 0.23 mmol), $Zn(OAc)_2 \cdot 2H_2O$ (0.53 g, 2.34 mmol). The crude product was

purified with column chromatography (silica gel, *n*-hexane/EtOAc, 6:1, v/v). The product was recrystallized from the mixture of eluent. The yield of red crystals was 0.07 g, 86%. $C_{24}H_{19}N_3$, MW = 349.44 g/mol, mp = 134-135 °C.

2,2'-(4,4'-(4-Methylphenylazanediyl)bis(4,1-phenylene)bis(methan-1-yl-1-ylidene))dimalononitrile (4) was obtained by the similar procedure as **1** using 4-[(4-formylphenyl)(4-methylphenyl)amino]benzaldehyde (**h**) (0.25 g, 0.78 mmol), malonodinitrile (0.11 g, 1.23 mmol), $Zn(OAc)_2 \cdot 2H_2O$ (0.53 g, 2.34 mmol). The crude product was purified with column chromatography (silica gel, *n*-hexane/EtOAc, 5:1, v/v). The target compound was recrystallized from the mixture of eluent. The yield of red crystals was 0.25 g, 87%. $C_{27}H_{17}N_5$, MW = 411.46 g/mol, mp = 202-203 °C.

3. RESULTS AND DISCUSSION

3.1. Synthesis and characterization

The intermediate compounds (**a-h**) were synthesized by the coupling and formylation reactions of the corresponding derivatives of triphenylamine (TPA) using the methods of Ullmann and Vilsmeier-Haack [36,37]. The target compounds (**1-4**) were prepared by Knoevenagel condensation of malonodinitrile with the different formyl derivatives of triphenylamine (**e-h**) in dehydrated *N*,*N*-dimethylformamide at room temperature with zinc acetate dihydrate as catalyst (Scheme 1). The chemical structures of compounds **1-4** were confirmed by IR, ^{1}H NMR, ^{13}C NMR, mass spectrometries and elemental analysis. They were found to be soluble in common organic solvents such as DCM, THF, acetone, DMF etc. The characteristic absorption bands of formyl groups observed at 1690 (C-O) and 2800 ((O)C–H) cm^{-1}, in the IR spectra of **e-h** dissappeared in the spectra of the target compounds **1-4** after the Knoevenagel condensation with the methylene group malonodinitrile. The characteristic bands of C≡N group appeared in the IR spectra **1-4** at 2222 cm^{-1} (for **1**), 2218 cm^{-1}

(for **2**), 2224 cm^{-1} (for **3**) and 2223 cm^{-1} (for **4**). This observation confirms that the malonodinitrile moieties are attached to TPA derivatives forming compounds **1-4**. In the ^{1}H NMR spectra of **1-4** the singlets of a proton of CH-C≡N appears at 7.59 (for **1**), 7.62 (for **2**), 7.68 (for **3**), 7.62 ppm (for **4**). The individual peaks in the ^{13}C NMR spectra of **1-4** are assigned to characteristic carbon atoms of C≡N moieties i.e. the singlets at 74.2 (for **1**), 78.1 (for **2**), 75.1 (for **3**), 78.1 ppm (for **4**). Mass spectra of all the synthesized compounds show the corresponding molecular ion peaks.

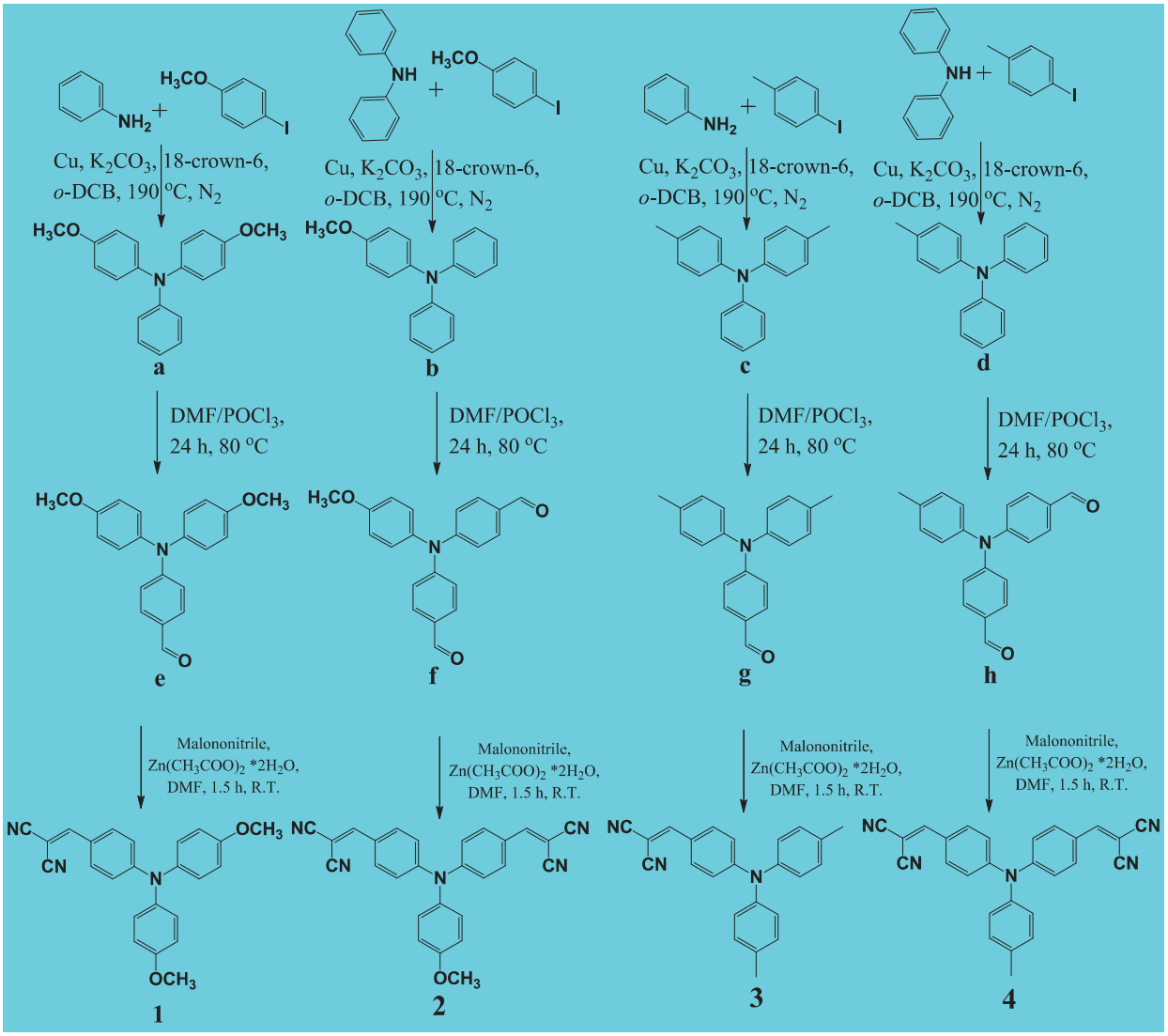

Scheme 1. Synthesis of triphenylamine based malonodinitriles **1-4**.

3.2. Thermal properties

The behavior under heating of compounds **1-4** was studied by DSC and TGA. The results are summarized in Table 1.

<Insert Table 1>

Compounds **1-4** showed moderately high thermal stability. Their 5% weight loss temperatures ($T_{ID-5\%}$) ranged from 284 to 323 °C. Compounds **1** and **3** with one dicyanovinyl moiety and two methoxy or methyl groups showed the higher thermal stability compounds **2** and **4** having two dicyanovinyl groups. Apparently, the thermal degradarion of these compounds starts from decomposition of dicyanovinyl moieties. Generally, compounds **1-4** showed lower $T_{ID-5\%}$ with respect of those of the derivatives of indandione and TPA [35].

After the synthesis, compounds **1-4** were obtained as crystalline substances showing melting signals (T_m) during the first heating scans. However they formed glasses when the melt samples were cooled down. In the second and the following DSC heating scans of the ccompounds neither melting nor crystallization signals were observed. For the illustration of the statement the DSC curves of compound **1** are shown in Fig. 1.

<Insert Figure 1>

Lower glass transition temperatures (T_g) of compound **1** and **3** having one dicyanovinyl moiety with respect of the corresponding compounds (**2** and **4**) having two dicyanovinyl moieties can apparently be explained by their lower molecular weights and by weeker intermolecular interaction. The values of T_g for the derivatives **1-4** are considerably lower in comparison with those of the earlier reported indandione-substituted derivatives of TPA [35].

3.3. Photophysical properties

The photophysical properties of compounds **1-4** were investigated by UV-vis absorption and fluorescence (FL) spectrometries. The absorption and FL spectra of dilute solutions and of the solid films of **1-4** are shown in Fig. 2, and the photophysical data are listed in Table 2.

<Insert Table 2>

<Insert Figure 2>

Dilute solutions of compounds **1-4** exhibited broad absorption bands covering the whole UV-vis range. The absorption bands in the high-energy region (220-370 nm) can be assigned to π-π* transitions. Absorptions bands appeared at ca. 390 nm present in the UV spectra of dilute solutions of **2** and **4** in THF can be attributed to the transitions involving two strong dicyanovinyl acceptor moieties. The absorption bands with λ_{max} around 443-485 nm correspond to intramolecular charge transfer (ICT) between the TPA donor part of the molecule and the accepting dicyanovinyl group. ICT absorption bands of dilute solutions of compounds **1-4** are red shifted by *ca.* 2-8 nm relative to those of the earlier reported derivatives of TPA and malonodinitrile having no methoxy or methyl substituents attached to TPA moieties [25]. Low-energy absorption bands of the solutions of compounds **2**, **4** in THF having two dicyanovinyl groups exhibit red-shift of almost 30 nm compared to those of the derivatives **1**, **3** containing single acceptor groups. The optical band gaps (E^g_{opt}) of compounds **1-4** estimated from the absorption edges of the dilute solutions were found to be in the short range of 2.35-2.48 eV. Absorption bands of the solid films of compounds **1-4** are broadened and red-shifted by 16-39 nm with respect of the spectra of the dilute solutions. The spectra of the films of compounds **2** and **4** having two dicyanovinyl groups exhibited longer shifts indicating more expressed ICT character in the solid state (Fig. 2). The values of E^g_{opt} of the solid samples of **1-4** were found to be by *ca.* 0.2 eV lower than those of dilute solutions and ranged from 2.16 to 2.23 eV.

FL spectra of dilute solutions of **1-4** in THF are shown in Fig. 2. The emission of the THF solutions of **1-4** appeared in the blue-yellow region with the intensity peaks in the range 547-580 nm. Fluorescence intensity maxima of the solutions of compounds **2** and **4** having two dicyanovinyl groups exhibited bathochromic shifts of with respect of those of compounds **1** and **3**, having single dicyanovinyl groups. This observation is consistent with the results of UV spectrometry. Compounds **1** and **3** showed larger Stokes shifts of 110 and 120 nm, respectively than compounds **2** and **4** (105 and 105 nm, respectively). This observation could be explained by the larger geometrical reorganizations of **1** and **3** after transition to the excited state. Fig. 2 shows the normalized emission spectra of the solid films of compounds **1-4**. The solid samples showed yellow-red emission peaking in the range of 621-637 nm. Compared with the FL spectra of the dilute solutions of compounds **1-4** in THF, their solid state spectra are red shifted by 53-74 nm apparently due to the processes associated with the formation of excimers in the solid state [38].

The values of Φ_F of the dilute solutions and of the solid layers of compounds **1-4** are given in Table 2. All the synthesized compounds showed low fluorescence quantum yields (Φ_F) in THF solutions. For the solid state samples they were found to be a little higher. In the solid state, π-conjugation of **1-4** is likely to be larger than that in the solution state due to the packing force. The extended π-conjugation provides larger Stokes shift in the solid state, which prevent reabsorption of the fluorescence [39]. That might be a possible reason for a little higher quantum yield of **1-4** in the solid state. Higher values of Φ_F ranging from 33.7 to 42.5% were observed for the solutions in toluene compared to those in chloroform and THF. This is probably due to the less pronounced ICT in toluene. ICT is considered to reduce Φ_F due to more pronounced relaxation and nonradiative decay of the excited states [40]. Low Φ_F of the solutions in chloroform can apparently be explained by the heavy atom effect of the solvent.

Φ_F of dilute THF solutions of compounds **1** and **3** containing one dicyanovinyl moiety and two methoxy or two methyl groups were found to be lower (0.3 and 2.3%, respectively) than those of the corresponding compounds **2** and **4** with two dicyanovinyl moieties and one methoxy or methyl groups

(1.7 and 5.2%, respectively). The solid films of compounds **2** and **4** containing two dicyanovinyl moieties and one methoxy or one methyl group also showed slighty higher quantum yields (Φ_F of 2.0 and 9.6%, respectively) than those of **1** and **3** with one dicyanovinyl moiety and two methoxy or methyl groups (Φ_F of 1.8 and 8.6%, respectively). Interestingly, compounds **3** and **4** with one or two methyl groups showed higher Φ_F than their metoxy-substituted analogues **1** and **2**.

3.4. Electrochemical and photoelectrical properties

The electrochemical properties of the solutions of TPA based malonodinitriles (**1-4**) in dichloromethane (DCM) were investigated by CV. The CV curves and differential pulse voltammperometric (DPV) spectra of **1-4** are shown in Fig. 3. The onset reduction and oxidation potentials *vs.* Fc together with the calculated values of the ionization potential (IP_{CV}) and electron affinity (EA_{CV}) are summarized in Table 3.

<Insert Table 3>

<Insert Figure 3>

CV studies of compounds **1** and **2** with two and one methoxy groups revealed one reversible and one irreversible oxidation peaks at 0.55 and 0.98 V for **1** and 0.66 and 1.13 V for **2** and one reduction peak at -1.75 V for **1** and two reduction peaks at -1.51 and -1.69 V for **2**. This observation can be attributed to the stepwise formation of radical dications upon oxidation and radical anions or dianions upon reduction. The irreversible oxidation peaks obsrved at 0.98 V for **1** and at 1.13 V for **2** can be attributed to oxidation of methoxy groups [39,41], causing radical recombination and formation of a quinoid structure [42]. The first oxidation onset for **1** was observed at the potential by 0.15 V lower than that observed for compound **2**, suggesting that compound **1** with two methoxy groups is oxidized easier than compound **2** with one methoxy group. Oxidation potential of compound **3** with two methyl

groups was found to be lower than that of compound **4** with one methyl group. These observations are in agreement with the previously reported data on the electrochemical properties of the derivatives of indandione and TPA [35]. Compounds **1** and **3** with two electron donating substituents (methoxy or methyl) exhibited more negative reduction potential values than compounds **2** and **4** with one electron donating substitutent (Fig. 3a).

Slightly lower IP_{CV} values were observed for methoxy-substituted compounds **1** and **2** (5.31, 5.46 eV, respectively) relative to those of methyl-substituted compounds **3** and **4** (5.49, 5.71 eV, respectively). The estimated EA_{CV} values for compounds **1-4** were found to be in the range of -3.41 – -3.05 eV. Compunds **2** and **4** having two dicyanovinylmoieties exhibited lower values of EA_{CV}**.** IP_{CV} and EA_{CV} values established for the derivatives of **1-4** are higher in comparison with those of the earlier reported derivatives of TPA and indandione [35].

DPV spectra of **1-4** (Fig. 3b) showed absolute peaks of oxidation and reduction processes. The first oxidation and first reduction process of **1-4** were helpful to determine their EA_{CV} and IP_{CV} values [43,44]. Compounds **2** and **4** containing two acceptor groups and one donor subsistuent have more positive oxidation potential values than compounds **1** and **3** with two donor substituents and one acceptor group. Reduction potential peaks are close for compounds with two donor groups **1** and **3** and for compounds with two acceptor groups **2** and **4**.

Ionization potentials of thin solid layers (IP_{EP}) of compounds **1-4** were estimated by photoelectron emission spectrometry. Photoelectron emission spectra and IP_{EP} of **1-4** are shown in Fig. 4. The IP_{EP} values of the layers of **1-4** were found to be rather close and ranged from 5.36 to 5.74 eV. Compounds **1** and **3** with two donor substituents exhibited a little lower IP_{EP} values than compounds **2** and **4** with two acceptor groups. Methoxy-susbtituted compounds **1** and **2** showed slightly lower IP_{EP} values (5.36, 5.53 eV, respectively) than the corresponding methyl-substituted counterparts **3** and **4** (5.55, 5.74 eV, respectively). These results are consistent with the results obtained by CV (Table 3).

<Insert Figure 4>

3.5. Computational studies

To get an insight into the molecular structures and electron distributions of compounds **1-4**, the geometries of the derivatives were optimized by using B3LYP hybrid functional and 6-31G* basis sets. The quantum-chemical calculations were performed using density functional theory (DFT) employed the Spartan'14 software [45]. The optimized structures and electronic distributions in the highest occupied molecular orbitals (HOMOs) and the lowest unoccupied molecular orbitals (LUMOs) of **1-4** are displayed in Fig. 5.

<Insert Figure 5>

HOMO of compounds **1-4** are delocalized mainly on the triphenylamino and on the electron deficient dicyanovinyl groups, whereas LUMO are distributed on dicyanovinyl groups and on the neighbouring aryl groups. Compounds **2** and **4** having two dicyanovinyl groups exhibit deeper HOMO and LUMO energy levels than compounds **1** and **3** having single acceptor groups. Slightly higher HOMO energy levels are observed for methoxy-substituted compounds **1** and **2** (-5.31, -5.94 eV, respectively) than for the corresponding methyl-substituted counterparts **3** and **4** (-5.49, -6.02 eV, respectively). The results of theoretical study are consistent with the results obtained by CV.

3.6. Charge-transporting properties

The photocurrent transients at different applied voltages for holes and electrons are shown in Fig. 6 and Fig. S2. They show highly dispersive charge transport and transit times (t_{tr}) could not be fixed in the linear plots of photocurrent versus time for the layers of methoxy-substituted compounds **1** and **2** (Fig. 6, Fig. S2, inserts). Clear intersections of two slopes were observed in the double-logarithmic

plots. To calculate charge mobilities, t_{tr} was determined from the intersection of the two slopes in the transient photocurrent curves. A clear shift of t_{tr} to the shorter times with increasing voltage indicated that the passage of photogenerated charges through the films was faster at higher electric fields. t_{tr} For the layers of methyl-substituted compounds **3** and **4** t_{tr} was not observed in the photocurrent transients, therefore it was not possible to estimated charge mobilities for these derivatives.

<Insert Figure 6>

The layers of methoxy-substituted compounds **1** and **2** showed the ambipolar charge transport properties. Fig. 7 shows the logarithmic charge mobility versus $E^{1/2}$ plots for hole and electron mobilities of in the layers of **1** and **2**. The hole mobility values of compounds **1** and **2** were in the range of 10^{-7} - 10^{-6} $cm^2/V{\cdot}s$. However, the electron mobility values of **1** and **2** were found to be considerably higher. They ranged from 4.53×10^{-5} $cm^2/V{\cdot}s$ (at electric field of 0.93×10^5 V/cm) to 4.56×10^{-4} $cm^2/V{\cdot}s$ (at electric field of $7.5{\cdot}10^5$ V/cm). Interestingly, electron mobility of **2** is by *ca.* an order of magnitude higher than that of conventional electron transporting materials tris (8-quinolinolato) aluminum (III), which is widely used in organic light emitting diodes [46].

<Insert Figure 7>

3.7. NLO properties

To obtain nonlinear refractive index and two photon absorption coefficients we used analytical expressions that can be derived using Gaussian decomposition method [47]. Open aperture data was fitted with the fallowing expression:

$$T_{OA}(z) = \sum_{m=0}^{\infty} \frac{\left[-\frac{q_0}{\left(1+\frac{z^2}{z_0^2}\right)}\right]^m}{(m+1)^{3/2}},$$

where z_0 is Reyleigh length and magnitude of two-photon absorption is characterized by coefficient:

$$q_0 = \alpha_2 \cdot I_0 \cdot L_{eff},$$

where L_{eff} is effective thickness of sample given by $L_{eff} = \frac{1 - e^{-\alpha \cdot L}}{\alpha}$, where L is the sample thickness.

Closed aperture measurements are affected by both Kerr and two photon absorption effects. To correctly estimate the magnitude of Kerr effect, closed aperture signal was divided by open aperture signal. Resulting data was fitted with fallowing expression:

$$T_{CA}(z) = \left(1 + \frac{4 \cdot \Delta\Phi \cdot \frac{z}{z_0}}{\left(\frac{z^2}{z_0^2} + 9\right)\left(\frac{z^2}{z_0^2} + 1\right)}\right),$$

where phase change of complex electrical field can be expressed as $\Delta\Phi = k \cdot n_2 \cdot I_0 \cdot L_{eff}$.

The example of experimental data is shown in Fig. 8.

<Insert Figure 8>

While carrying out measurements, we concluded that selected organic compounds do not exhibit significant (detectable) two photon absorption at the wavelength of 1064 nm.

Using experimentally obtained nonlinear refractive index values n_2 we have acquired the real part of third-order susceptibility using the following expression [48]:

$$\chi_{Re}^{(3)}(esu) = \left(4 \cdot \frac{\varepsilon_0 \cdot c \cdot {n_0}^2}{3}\right) \cdot n_2\left(\frac{m^2}{W}\right),$$

where λ is laser wavelength, ε_0 is vacuum dielectric constant, n_0 is refractive index and c is speed of light in vacuum. The acquired values are presented in Table 4.

<Insert Table 4>

Additionally, quantum chemical calculations of isotropically averaged molecular second-order hyperpolarizability real part γ_A were carried out using CPKS method in Gaussian 09. For the

comparison of experimental values with predictions by quantum chemical calculations, we have to recalculated experimental values of third-order susceptibility to real part of second-order hyperpolarizability γ_E by the following expression [49]:

$$\gamma_E = \frac{\chi_{Re}^{(3)}}{\left[\frac{1}{3}\left(n_0{}^2 + 2\right)\right]^4 \cdot N},$$

where N is molecule concentration per cm^3. Recalculated values are presented in Table 4. Experimentally measured values have a good correlation with quantum chemistry calculations (see Fig. 9). At the same time one could notice that the calculations yielded *ca.* 4 times larger values of second-order hyperpolarizability. All molecules had positive sign for second order hyperpolarizability. Compared to nonlinear refractive index of triphenylamine [50], they have the same sign but the values are by one order of magnitude larger.

<Insert Figure 9>

To analyze the results, the studied molecules were divided in two groups i.e. molecules with A-D structure (**1**, **3**) and molecules with A-D-A structure (**2**, **4**). In the first pare the strength of donor group was increased by replacing methyl groups with methoxy groups (cf. compounds **1** and **3**). The experimental results and quantum chemistry calculations showed that this replacement lead to the decrease of second order hyperpolarizability. To better understand why such effect was observed we compared the angles between the acceptor arm and the central NC_3 group (further in the text central plane). We observed that the angle between acceptor group plane and central plane is around 15-20°. This observation allows us to believe that electrons can freely transit from central plane to acceptor group. In this case, the angle between phenyl groups containing either methyl or methoxy substituents and the central plane affects second order hyperpolarizability. For **1** the angle was around 68°, while for **3** it was 63°. The experimental results show that smaller angle leads to larger second order hyperpolarizability.

For the second group (compounds **2** and **4**) we concluded that by the attachement of methoxy group, the second order hyperpolarizability increased. For these molecules none of the phenyl groups were close to being in one plane with central group. In this case we believe that second order hyperpolarizability is more influenced by the strength of donor and acceptor groups. The experimental results show that for the compound with stronger donor group, the second order hyperpolarizability is larger.

4. CONCLUSIONS

The derivatives of triphenylamine containing the different numbers of electron-accepting dicyanovinyl and electron-donating methoxy or methyl groups were obtained by the Knoevenagel condensation reaction. The synthesized compounds form molecular glasses with glass transition temperatures ranging from 38 to 107 ^{o}C. Their 5% weight loss temperatures range from 284 to 323 ^{o}C. The absorption spectra of the dilute solutions of the compounds showed absorption maxima in the range 443-485 nm correspond to intramolecular charge transfer. The emission spectra of the compounds exhibited positive solvatochromic effect, and changing from the solutions in toluene to those in THF they showed bathochromic shifts of emission maxima. Cyclic voltammetry revealed close values of the solid state ionization potentials ranging from 5.31 to 5.71 eV, and electron affinities ranging from -3.05 to -3.41. The hole mobility values of methoxy-substituted compounds were in the range of 10^{-7} - 10^{-6} cm^2/V·s while electron mobility values reached 4.56×10^{-4} cm^2/V·s at electric field of 7.5×10^{5} V/cm. All the molecules had positive sign for second order hyperpolarizability. The smaller angle between the central plane of triphenylamino group and dicyanovinyl substituents resulted in larger second order hyperpolarizability. The second order hyperpolarizability was larger for the compounds having methoxy groups as compared with those containing methyl substituents.

Acknowledgments

This research was supported by H2020-ICT-2014/H2020-ICT-2014-1 project PHEBE (grant agreement No 641725) and by the National Research program IMIS2 project "Photonics and Materials for Photonics". Support of the Lithuanian Academy of Sciences is gratefully acknowledged.

Appendix A. Supplementary data

Supplementary data related to this article can be found at http:// dx.doi.org.

REFERENCES

[1] Grucela-Zajac M, Bijak K, Kula S, Filapek M, Wiacek M, Janeczek H, et al. (Photo)physical properties of new molecular glasses end-capped with thiophene rings composed of diimide and imine units. J Phys Chem C 2014;118:13070–86.

[2] Yu Y, Jiao B, Wu Z, Li Z, Ma L, Zhou G, et al. Fluorinated 9,9′-bianthracene derivatives with twisted intramolecular charge-transfer excited states as blue host materials for high-performance fluorescent electroluminescence. J Mater Chem C 2014;2:9375-84.

[3] Greulich TW, Suzuki N, Daniliuc CG, Fukazawa A, Yamaguchi E, Studer A, et al. A biphenyl containing two electron-donating and two electron-accepting moieties: a rigid and small donor–acceptor–donor ladder system. Chem Commun 2016;52:2374-7.

[4] Crossley DL, Cade IA, Clark ER, Escande A, Humphries MJ, King SM, et al. Turner, enhancing electron affinity and tuning band gap in donor–acceptor organic semiconductors by benzothiadiazole directed C–H borylation. Chem Sci 2015;**6**:5144-51.

[5] Sirringhaus H. Organic semiconductors: An equal-opportunity conductor. Nat Mater 2003;2:641-2.

[6] Lee W, Cho N, Kwon J, Ko J, Hong JI. New organic dye based on a 3,6-disubstituted carbazole donor for efficient dye-sensitized solar cells. Chem Asian J 2012;7:343-50.

[7] Iwan A, Sek D. Polymers with triphenylamine units: Photonic and electroactive materials. Prog Polym Sci 2011;36:1277-325.

[8] Gudeika D, Grazulevicius JV, Volyniuk D, Juska G, Jankauskas V, Sini G. Effect of ethynyl linkages on the properties of the derivatives of triphenylamine and 1,8-naphthalimide. J Phys Chem C 2015;119:28335-46.

[9] Hua JL, Li B, Meng FS, Ding F, Qian SX, Tian H. Two-photon absorption properties of hyperbranched conjugated polymers with triphenylamine as the core. Polymer 2004;45:7143-9.

[10] Huang JH, Su JH, Li X, Lam MK, Fung KM, Fan HH, et al. Bipolar anthracene derivatives containing hole- and electron-transporting moieties for highly efficient blue electroluminescence devices. J Mater Chem 2011;21:2957-64.

[11] Xu L, Zhao Y, Long G, Wang Y, Zhao J, Li D, et al. Synthesis, structure, physical properties and OLED application of pyrazine–triphenylamine fused conjugated compounds. RSC Adv 2015:5;63080-6.

[12] Yang Z, Wang D, Bai X, Shao C, Cao D. Designing triphenylamine derivative dyes for highly effective dye-sensitized solar cells with near-infrared light harvesting up to 1100 nm. RSC Adv 2014;4:48750-7.

[13] Song Y, Di C, Xu W, Liu Y, Zhang D, Zhu D. New semiconductors based on triphenylamine with macrocyclic architecture: synthesis, properties and applications in OFETs. J Mater Chem 2007;17:4483-91.

[14] Shirota Y, Kageyama H. Charge carrier transporting molecular materials and their applications in devices. Chem Rev 2007;107:953-1010.

[15] Li Y, Xue L, Xia H, Xu B, Wen S, Tian W. Synthesis and properties of polythiophene derivatives containing triphenylamine moiety and their photovoltaic applications. J Polym Sci Pol Chem 2008;46:3970–84.

[16] Tang S, Li W, Shen F, Liu D, Yang B, Ma Y. Highly efficient deep-blue electroluminescence based on the triphenylamine-cored and peripheral blue emitters with segregative HOMO−LUMO characteristics. J Mater Chem 2012;22:4401−8.

[17] Jiang P, Zhao DD, Yang XL, Zhu XL, Chang J, Zhu HJ. Blue-light-emitting multifunctional triphenylamine-centered starburst quinolines: synthesis, electrochemical and photophysical properties. Org Biomol Chem 2012;10:4704−11.

[18] Chiu KY, Su TX, Li JH, Lin TH, Liou GS, Cheng SH. Novel trends of electrochemical oxidation of amino-substituted triphenylamine derivatives. J Electroanal Chem 2005;575:95–101.

[19] (a) Fuks-Janczarek I, Nunzi JM, Sahraoui B, Kityk IV, Berdowski J, Caminade AM, et al. Third-order nonlinear optical properties and two-photon absorption in branched oligothienylenevinylenes. Opt Commun 2002;209:461-6; (b) Iliopoulos K, El-Ghayoury A, El Ouazzani H, Pranaitis M, Belhadj E, Ripaud E, et al. Nonlinear absorption reversing between an electroactive ligand and its metal complexes. Optics Express 2012;20;25311-6; (c) Sahraoui B, Luc J, Meghea A, Czaplicki R, Fillaut JL, Migalska-Zalas A. Nonlinear optics and surface relief gratings in alkynyl–ruthenium complexes. J Opt A: Pure Appl Opt 2009;11:1-26; (d) Kulyk B, Guichaoua D, Ayadi A, El-Ghayoury A, Sahraoui B. Metal-induced efficient enhancement of nonlinear optical response in conjugated azo-based iminopyridine complexes. Org Electron 2016;36:1-6.

[20] (a) Dalton LR, Sullivan PA, Bale DH. Electric field poled organic electro-optic materials: state of the art and future prospects. Chem Rev 2010;110:25-55; (b) Kulyk B, Taboukhat S, Akdas-Kilig H, Fillaut JL, Boughaleb Y, Sahraou B. Nonlinear refraction and absorption activity of dimethylaminostyryl substituted BODIPY dyes. RSC Adv 2016;6:84854-9.

[21] (a) Luo J, Zhou XH, Jen AKY. Rational molecular design and supramolecular assembly of highly efficient organic electro-optic materials. J Mater Chem 2009;19:7410-24; (b) Sahraoui B, Rivoire G,

Terkia-Derdra N, Sallé M, Zaremba J. Third-order nonlinear optical properties of new bisdithiafulvenyl-substituted tetrathiafulvalene. J Opt Soc Am B 1998;15:923-8; (c) El Ouazzani H, Iliopoulos K, Pranaitis M, Krupka O, Smokal V, Kolendoand A, et al. Second- and third-order nonlinearities of novel push-pull azobenzene polymers. J Phys Chem B 2011;115:1944-9.

[22] Kober S, Salvador M, Meerholz K. Organic photorefractive materials and applications. Adv Mater 2011;23:4725-63.

[23] Jialing Lu, Jianyu Yuan, Wenping Guo, Xiaodong Huang, Zeke Liu, Haibing Zhao, et al. Effects of cyano (CN)-groups on the planarity, film morphology and photovoltaic performance of benzodithiophene-based polymers. Polym Chem 2014;5:4772-80.

[24] Tancini F, Wu YL, Schweizer WB, Gisselbrecht JP, Boudon C, Jarowski PD, et al. 1,1-Dicyano-4-[4-(diethylamino)phenyl]buta-1,3-dienes: structure–property relationships. Eur J Org Chem 2012;14:2756–65.

[25] Yang Y, Li B, Zhang L. Design and synthesis of triphenylamine-malonitrile derivatives as solvatochromic fluorescent dyes. Sensor Acuat B Chem 2013;183:46–51.

[26] Wraight CA, Vakkasoglu AS, Poluektov Y, Mattis AJ, Nihan D, Lipshutz BH. The 2-methoxy group of ubiquinone is essential for function of the acceptor quinones in reaction centers from Rba. Sphaeroides. Biochim Biophys Acta 2008;1777:631–6.

[27] Gagne RR, Koval CA, Lisensky GC. Ferrocene as an internal standard for electrochemical measurements. Inorg Chem 1980;19:2854-5.

[28] Miyamoto E, Yamaguchi Y, Yokoyama M. Ionization potential of organic pigment film by atmospheric photoelectron emission analysis. Denshishashin Gakkai-shi (Electrophotography) 1989;28:364-70.

[29] Gudeika D, Grazulevicius JV, Volyniuk D, Butkute R, Juska G, Miasojedovas A, et al. Structure-properties relationship of the derivatives of carbazole and 1,8-naphthalimide: effects of the substitution and the linking topology. Dyes Pigm 2015;114:239-52.

[30] Lukstaite J, Gudeika D, Grazulevicius JV, Grigalevicius S, Zhang B, Xie Z. Copolymers containing electronically isolated indolyl fragments as materials for optoelectronics. React Funct Polym 2010;70:572-7.

[31] Gudeika D, Volyniuk D, Grazulevicius JV, Skuodis E, Yu SY, Liou WT, et al. Derivative of oxygafluorene and di-tert-butyl carbazole as the host with very high hole mobility for high-efficiency blue phosphorescent organic light-emitting diodes. Dyes Pigm 2016;130:298-305.

[32] Staskun B. Conversion of triphenylamine and acylated triphenylamines into 9,10-diaryl-9-acridanols. J Org Chem 1968;33:3031-6.

[33] Marsden RJB, Schönberg A, Michaelis R. Notes. J Chem Soc 1937:627-8.

[34] Liu YH, Chen C, Yang LM. Diazabutadiene: a simple and efficient ligand for copper-catalyzed N-arylation of aromatic amines. Tetrahedron Lett 2006;47:9275–8.

[35] Zilinskaite V, Gudeika D, Grazulevicius JV, Volyniuk D, Buika G, Jankauskas V, et al. Derivatives of indandione and differently substituted triphenylamine with charge-transporting and NLO properties. Dyes Pigm 2015;114:239-52.

[36] Ullmann F. Ueber eine neue bildungsweise von diphenylaminderivaten. Ber Dtsch Chem Ges 1903;36:2382-4.

[37] Vilsmeier V, Haack A. Über die einwirkung von halogenphosphor auf alkyl-formanilide. Eine neue methode zur darstellung sekundärer und tertiärerp-alkylamino-benzaldehyde. Ber Dtsch Chem Ges 1927;60:119-22.

[38] Lupton JM, Samue IDW, Burn PL. Origin of spectral broadening in p-conjugated amorphous semiconductors. Phys Rew B 2002;66:155206-11.

[39] Katoh R, Suzuki K, Furube A, Kotani M, Tokumaru K. Fluorescence quantum yield of aromatic hydrocarbon crystals. J Phys Chem C 2009;113:2961-5.

[40] Gudeika D, Grazulevicius JV, Volyniuk D, Juska G, Jankauskas V, Sini G. Effect of ethynyl linkages on the properties of the derivatives of triphenylamine and 1,8-naphthalimide. J Phys Chem C 2015;119:28335-46.

[41] Gudeika D, Grazulevicius JV, Sini G, Bucinskas A, Jankauskas V, Miasojedovas A, et al. S. New derivatives of triphenylamine and naphthalimide as ambipolar organic semiconductors: experimental and theoretical approach. Dyes Pigm 2014;106:58–70.

[42] Hsiao SH, Liou GYS, Kung YC, Hsiung TJ. Synthesis and properties of new aromatic polyamides with redox-active 2,4-dimethoxytriphenylamine moieties. J Polymer Sci Polymer Chem 2010;48:3392–401.

[43] DAndrade BW, Datta S, Forrest SR, Djurovich P, Polikarpov E, Thompson ME. Relationship between the ionization and oxidation potentials of molecular organic semiconductors. Org Electron 2005;6:11–20.

[44] Ahmad J, Astin KB. Correlation of reduction potentials of cyanine dyes with their orbital energies. Dyes Pigm 1988;9:3217-20.

[45] Spartan'14 for windows version 1.1.2. 1840 Von Karman Avenue, Suite 370, Irvine, CA.

[46] Naka S, Okada H, Onnagawa H, Yamaguchi Y, Tsutsui T. Carrier transport properties of organic materials for EL device operation. Synth Met 2000;111:331–3.

[47] Bahae MS, Said AA, Wei TH, Hagan DJ, Van Stryland EW. Sensitive measurements of optical nonlinearities using a single beam. IEEE J Quantum Electron 1990;26:760–9.

[48] del Coso R, Solis J. Relation between nonlinear refractive index and third-order susceptibility in absorbing media. J Opt Soc Am B 2004;21:640-4.

[49] Sharafudeen KN, Adithya A, Vijayakumar S, Sudheesh P, Kalluraya B, Chandrasekharan K. Multiphoton absorption process and self-focusing effect in coumarin derivative doped PMMA films by Z-scan and optical limiting studies. Curr Appl Phys 2011;11:1089–93.

[50] Bundulis A, Nitiss E, Mihailovs I, Busenbergs J, Rutkis M. Study of structure-third-order susceptibility relation of indandione derivatives. J Phys Chem C 2016;120:27515-22.

Scheme 1. Synthesis of triphenylamine based malonodinitriles **1-4**.

Table 1. Thermal characteristics of compounds **1-4**.

Table 2. Absorption and emission characteristics of the solutions of **1-4** in various solvents and of the solid films.

Table 3. Electrochemical and photoelectrical characteristics of compounds **1-4**.

Table 4. Experimental values of nonlinear refractive index n_2, the real part of third-order susceptibility χ_{Re} and second-order hyperpolarizability γ_E, as well as the results of quantum chemistry calculations of second order hyperpolarizability γ_A.

Figure 1. DSC thermograms of compound **1** (scan rate of 10 ºC/min, N_2 atmosphere).

Figure 2. (a) Normalized absorption, FL spectra of dilute solutions of **1-4** in THF (10^{-5} M); (b) absorption and normalized FL spectra of solid films of **1-4**. The wavelengths of low-energy absorption maxima were used as excitation wavelengths.

Figure 3. (a) CV of **1-4** (c = 10^{-6} M) recorded in the inert atmosphere. Scan rate 100 mV s^{-1}, electrolyte 0.1 M Bu_4NPF_6 in DCM; (b) DPV curves of 1mM of the solutions of compounds **1-4** in 1M Bu_4NBF_6 in DCM electrolyte.

Figure 4. Photoelectron emission spectra of the solid films of compounds **1-4**.

Figure 5. Frontier orbital plots for compounds **1-4**.

Figure 6. Photocurrent transients for holes of compound **2** (a) and for electrons of compound **2** (b) in log-log scales. The arrows indicate t_{tr} for two different electric fields. In the inserts, photocurrent transients in the linear scales are shown.

Figure 7. Electric field dependences of hole and electron mobilities of the layers of compounds **1** and **2** recorded at room temperature.

Figure 8. Experimental data. Kerr effect data were acquired by dividing closed aperture data with open aperture data.

Figure 9. Experimental and theoretical values of second order hyperpolarizability.

Scheme

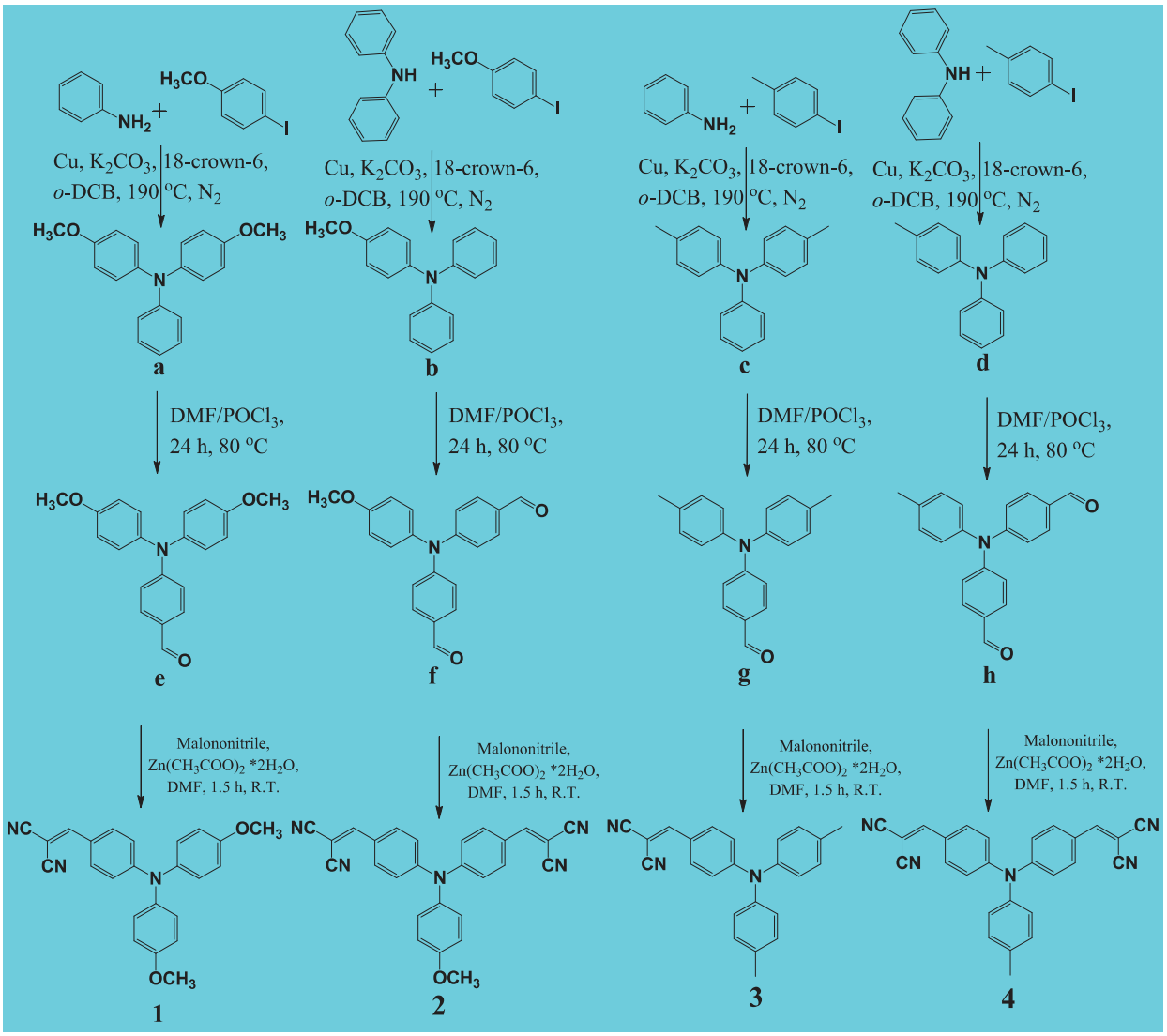

Scheme 1. Synthesis of triphenylamine based malonodinitriles **1-4**.

List of Tables

Table 1. Thermal characteristics of compounds **1-4**.

Compound	T_m, [°C][a]	T_g, [°C][b]	$T_{ID-5\%}$, [°C][c]
1	142	38	307
2	152	51	284
3	138	85	323
4	207	107	297

[a] Scan rate 10 °C/min, N_2 atmosphere, T_g - glass-transition temperature, T_m - melting temperature. [b] Second heating scan. [c] Scan rate 20 °C/min, N_2 atmosphere, $T_{ID-5\%}$ - 5% weight loss temperature.

Table 2. Absorption and emission characteristics of the solutions of **1-4** in various solvents and of the solid films.

Compound		Solvent			
		Toluene	Chloroform	THF	Solid film
1	λ_{abs} [a], nm	444	450	437	453
	λ_{em} [b], nm	529	540	547	621
	Φ_F [c], %	35.2	0.7	0.3	1.8
	Stokes shift, nm	85	90	110	168
2	λ_{abs} [a], nm	474	485	472	503
	λ_{em} [b], nm	556	565	580	633
	Φ_F [c], %	33.7	1.9	1.7	2.0
	Stokes shift, nm	82	80	108	130
3	λ_{abs} [a], nm	443	452	438	454
	λ_{em} [b], nm	528	542	558	628
	Φ_F [c], %	42.5	4.9	2.3	8.6
	Stokes shift, nm	85	90	120	174
4	λ_{abs} [a], nm	472	482	468	505
	λ_{em} [b], nm	548	557	573	637
	Φ_F [c], %	38.7	6.8	5.7	9.6
	Stokes shift, nm	76	75	105	132

[a] Peak wavelength of absorption bands. [b] Wavelength at fluorescence band maximum. [c] FL quantum yield.

Table 3. Electrochemical and photoelectrical characteristics of compounds **1-4**.

Compound	$E_{onset}^{ox_1}$ / $E_{onset}^{ox_2}$ *vs* Fc/V	$E_{onset}^{red_1}$ / $E_{onset}^{red_2}$ *vs* Fc/V	IP_{CV} /eV[a]	EA_{CV} /eV[a]	IP_{EP} /eV[b]	E_g^{op} /eV[c]	E_g^{op} /eV[d]	E_g^{el} /eV[e]
1	0.51/0.98	-1.75	5.31	-3.05	5.36	2.38	2.16	2.26
2	0.66/1.13	-1.51/-1.69	5.46	-3.29	5.53	2.35	2.21	2.17
3	0.69/-	-1.69	5.49	-3.11	5.55	2.48	2.23	2.38
4	0.91/-	-1.39/-1.62	5.71	-3.41	5.74	2.40	2.20	2.30

[a] $IP_{CV} = -(E_{onset}^{ox_1} + 4.8)$; $EA_{CV} = -(E_{onset}^{red_1} + 4.8)$ (where, $E_{onset}^{red_1}$ and $E_{onset}^{ox_1}$ are onset reduction and oxidation potentials *versus* the Fc^+/Fc); [b] IP_{EP} - ionization potentials of thin solid layers; [c] $E_g^{op} = 1240/\lambda_{edge}$, in which the λ_{edge} is the onset value of absorption spectrum of dilute DCM solution in long wave direction; [d] E_g^{op} for solid film; [e] $E_g^{el} = IP_{CV} - EA_{CV}$.

Table 4. Experimental values of nonlinear refractive index n_2, the real part of third-order susceptibility χ_{Re} and second-order hyperpolarizability γ_E, as well as the results of quantum chemistry calculations of second order hyperpolarizability γ_A.

Compound	n_2, cm^2/W	χ_{Re}, esu	γ_E, esu	γ_A, esu
TPA	$(8.6\pm2.9)\cdot10^{-14}$	$(4.5\pm1.5)\cdot10^{-12}$	$(16.9\pm5.7)\cdot10^{-35}$	$5.8\cdot10^{-35}$
1	$(111.9\pm9.5)\cdot10^{-15}$	$(13.7\pm1.2)\cdot10^{-12}$	$(22.1\pm1.9)\cdot10^{-34}$	$5.20\cdot10^{-34}$
2	$(19.7\pm3.0)\cdot10^{-14}$	$(24.2\pm3.6)\cdot10^{-12}$	$(36.7\pm5.5)\cdot10^{-34}$	$10.4\cdot10^{-34}$
3	$(21.3\pm2.1)\cdot10^{-14}$	$(26.1\pm2.5)\cdot10^{-12}$	$(40.0\pm3.9)\cdot10^{-34}$	$9.80\cdot10^{-34}$
4	$(13.4\pm1.8)\cdot10^{-14}$	$(16.5\pm2.2)\cdot10^{-12}$	$(20.3\pm2.7)\cdot10^{-34}$	$4.60\cdot10^{-34}$

List of Figures

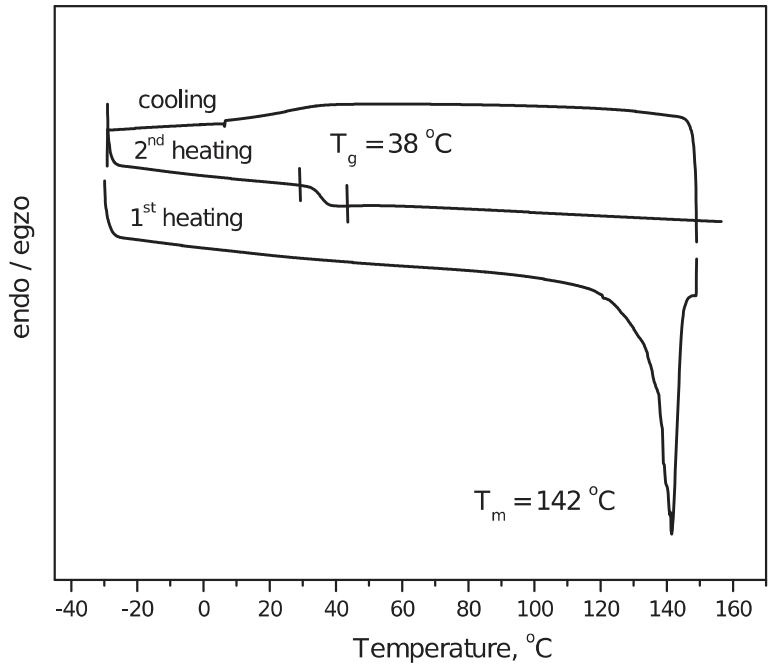

Figure 1. DSC thermograms of compound **1** (scan rate of 10 ºC/min, N_2 atmosphere).

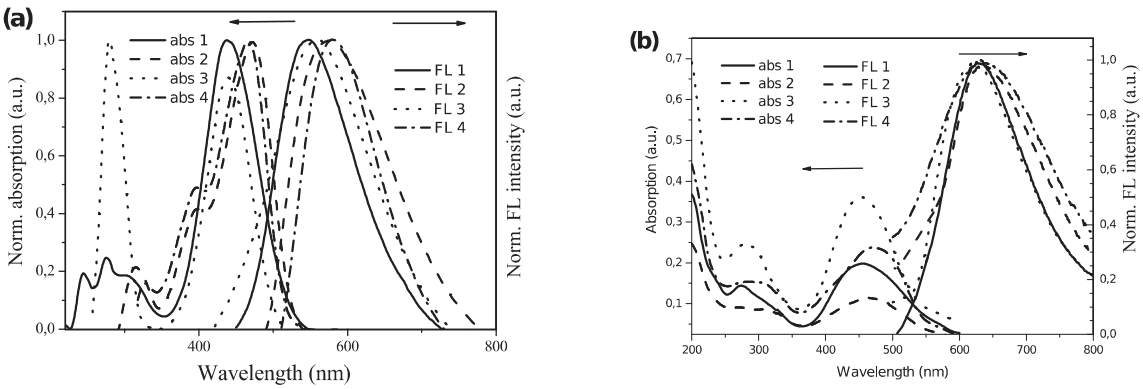

Figure 2. (a) Normalized absorption, FL spectra of dilute solutions of **1-4** in THF (10^{-5} M); (b) absorption and normalized FL spectra of solid films of **1-4**. The wavelengths of low-energy absorption maxima were used as excitation wavelengths.

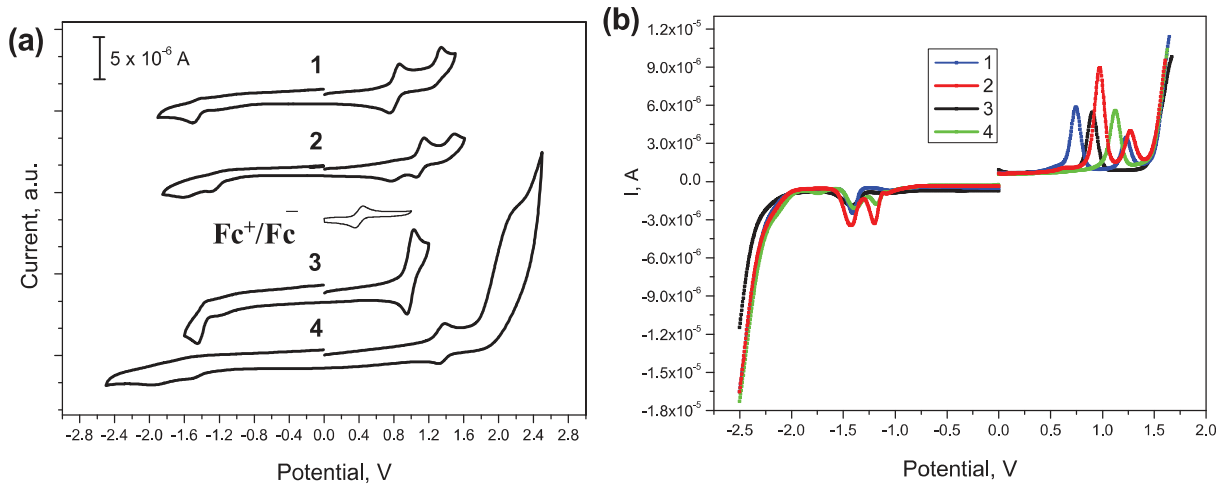

Figure 3. (a) CV of **1-4** (c = 10^{-6} M) recorded in the inert atmosphere. Scan rate 100 mV s^{-1}, electrolyte 0.1 M Bu_4NPF_6 in DCM; (b) DPV curves of 1mM of the solutions of compounds **1-4** in 1M Bu_4NBF_6 in DCM electrolyte.

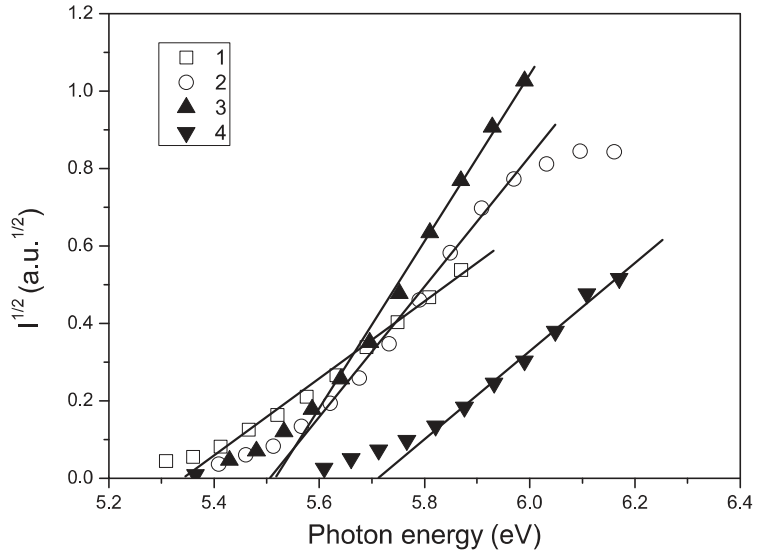

Figure 4. Photoelectron emission spectra of the solid films of compounds **1-4**.

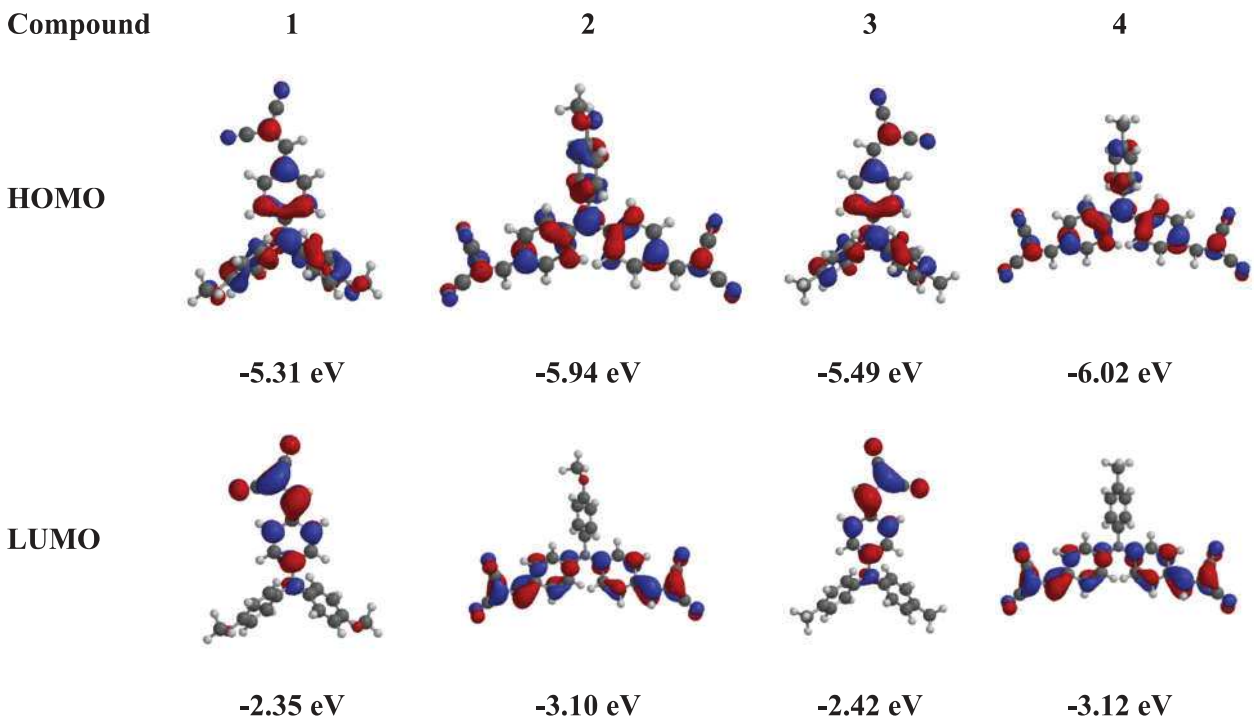

Figure 5. Frontier orbital plots for compounds **1-4**.

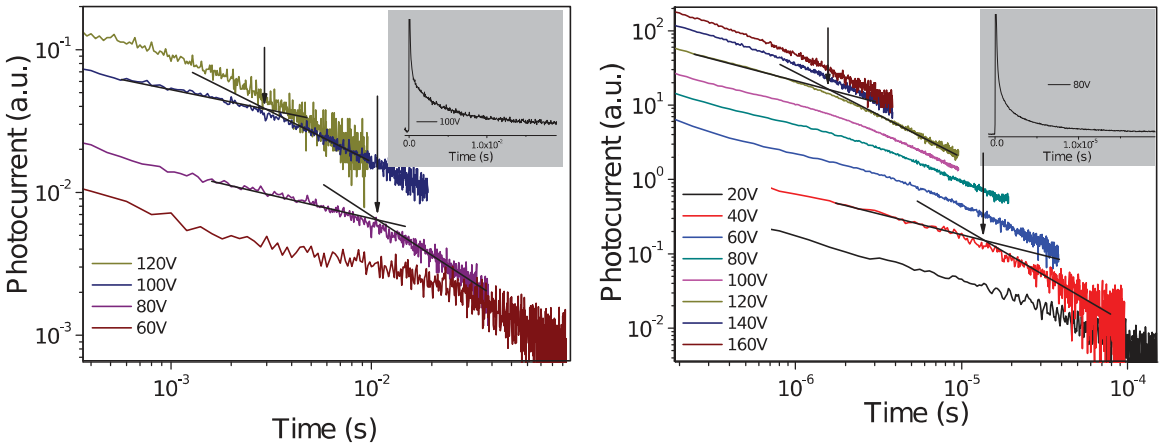

a) b)

Figure 6. Photocurrent transients for holes of compound **2** (a) and for electrons of compound **2** (b) in log-log scales. The arrows indicate t_{tr} for two different electric fields. In the inserts, photocurrent transients in the linear scales are shown.

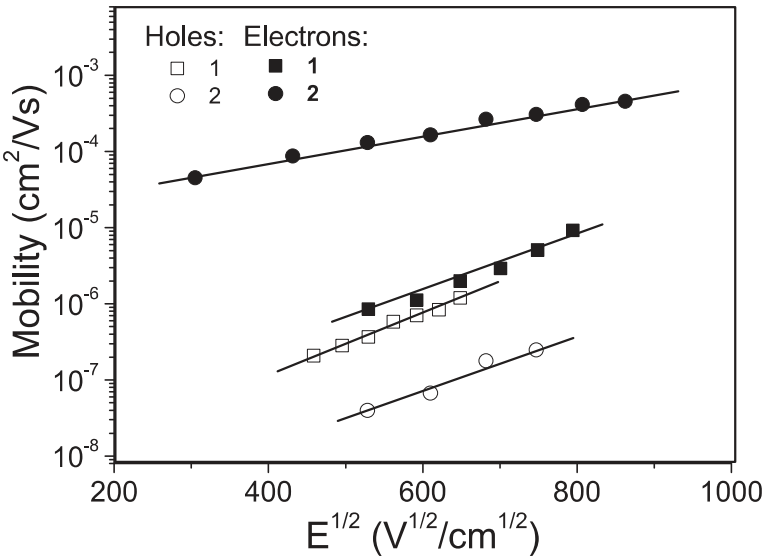

Figure 7. Electric field dependences of hole and electron mobilities of the layers of compounds **1** and **2** recorded at room temperature.

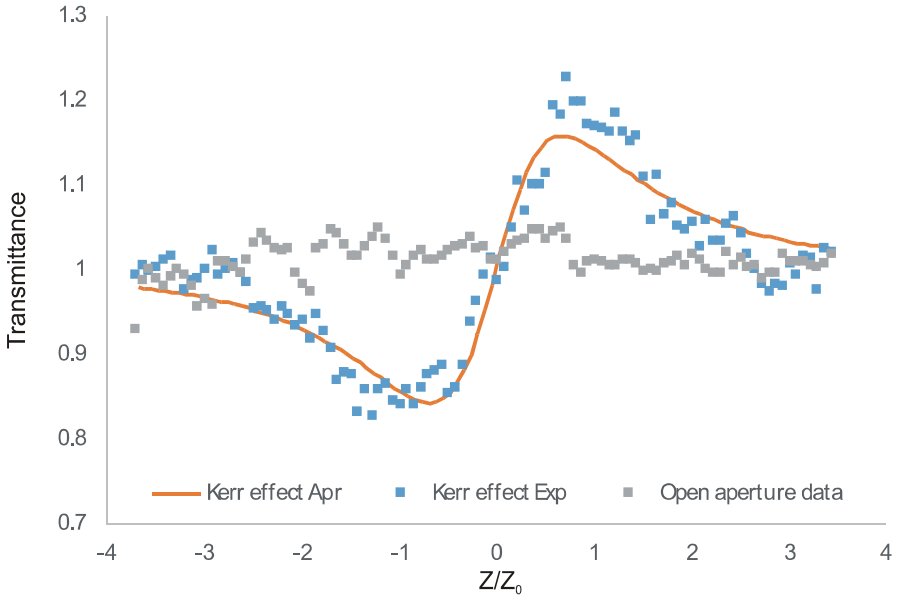

Figure 8. Experimental data. Kerr effect data were acquired by dividing closed aperture data with open aperture data.

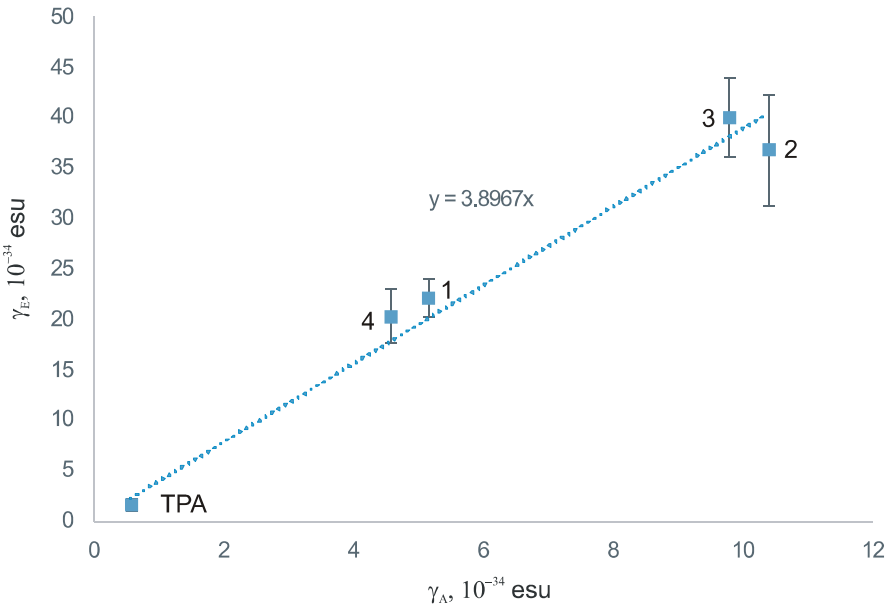

Figure 9. Experimental and theoretical values of second order hyperpolarizability.

Supporting Information

Donor and acceptor substituted triphenylamines exhibiting bipolar charge-transporting and NLO properties

Dalius Gudeika[1], Arturs Bundulis[2], Igors Mihailovs[2], Dmytro Volyniuk[1], Juozas V. Grazulevicius[1], Martins Rutkis[2]

[1] *Department of Organic Technology, Kaunas University of Technology, Radvilenu pl. 19, LT- 50254, Kaunas, Lithuania*

[2] *Institute of Solid State Physics, University of Latvia, 8 Kengaraga St., Riga LV-1063, Latvia*

Corresponding author. E-mail address: juogra@ktu.lt (Juozas Vidas Gražulevičius)

Characterization of compounds 1-4

2-(4-(Bis(4-methoxyphenyl)amino)benzylidene)malononitrile (1). ^{1}H NMR (700 MHz, $CDCl_3$, δ, ppm): 7.81 (d, 4H, *J* = 8.9 Hz, Ar), 7.59 (s, 1H, CH), 7.17 (d, 4H, *J* = 8.9 Hz, Ar), 7.10 (d, 2H, *J* = 8.9 Hz, Ar), 6.95 (d, 2H, *J* = 8.9 Hz, Ar), 3.86 (s, 6H, OCH_3). ^{13}C NMR (176 MHz, $CDCl_3$, δ, ppm): 156.2, 145.7, 131.8, 128.8, 127.7, 125.9, 121.7, 117.8, 115.7, 113.4, 74.2, 55.8. IR (KBr), ν, cm^{-1} 3143 ($C\text{-}H_{ar}$), 2959, 2840 ($C\text{-}H_{aliph}$), 1574, 1557 (C=C), 2222 (C≡N), 1495, 1456, 1421 (OCH_3), 1328, 1311, 1294 (C-N), 1183 (C-O-C), 830 ($C\text{-}H_{ar}$); MS ($APCI^+$, 20 V), m/z: 381 ($[M]^+$). Anal. Calcd for $C_{24}H_{19}N_3O_2$ (%): C, 75.57; H, 5.02; N, 11.02; O, 8.39. Found (%): C, 75.52, H, 5.08, N, 11.09.

2,2'-(4,4'-(4-Methoxyphenylazanediyl)bis(4,1-phenylene)bis(methan-1-yl-1-ylidene))dimalononitrile (2) ^{1}H NMR (700 MHz, $CDCl_3$, δ, ppm): 7.83 (d, *J* = 8.9 Hz, 4H), 7.62 (s, 2H, CH), 7.16 (d, 4H, *J* = 8.9 Hz, Ar), 7.11 (d, 2H, *J* = 8.9 Hz, Ar), 6.97 (d, 2H, *J* = 8.9 Hz, Ar), 3.85 (s, 3H, OCH_3). ^{13}C NMR (176 MHz, $CDCl_3$, δ, ppm): 158.9, 151.4, 136.7, 132.7, 129.4, 125.6, 122.2,

115.8, 114.4, 113.3, 78.1, 55.6. IR (KBr), ν, cm^{-1}: 3007 (C-H_{ar}), 292, 2833 (C-H_{aliph}), 2218 (C≡N), 1502 (C=C), 1342, 1274 (C-N), 1246, 1175 (C-O-C), 829 (C-H_{ar}); MS (APCI$^+$, 20 V), m/z: 427 ([M]$^+$). Anal. Calcd for $C_{27}H_{17}N_5O$ (%): C, 75.86; H, 4.01; N, 16.38; O, 3.41. Found (%): C, 75.87, H, 4.05, N, 16.32.

2-(4-(Bis(4-methylphenyl)amino)benzylidene)malononitrile (3). ^{1}H BMR (700 MHz, $CDCl_3$, δ, ppm): 7.72 (d, 2H, *J* = 9.1 Hz, Ar), 7.68 (s, 1H, CH), 7.62 (d, 2H, *J* = 8.7 Hz, Ar), 7.53 (d, 2H, *J* = 8.7 Hz, Ar), 7.36-7.34 (m, 6H, Ar), 2.20 (s, 6H, CH_3). ^{13}C NMR (176 MHz, $CDCl_3$, δ, ppm): 155.3, 148.5, 135.1, 129.5, 127.7, 125.5, 124.5, 118.7, 116.9, 113.4, 75.1, 34.8. IR (KBr), ν, cm^{-1}: 3023 (C-H_{ar}), 2922, 2855 (C-$H_{aliph.}$), 2224 (C≡N), 1569, 1500, 1545 (C=C), 1333, 1318, 1301 (C-N), 815 (C-H_{ar}); MS (APCI$^+$, 20 V), m/z: 349 ([M]$^+$). Anal. Calcd for $C_{24}H_{19}N_3$ (%): C, 82.49; H, 5.48; N, 12.03. Found (%): C, 82.46, H, 5.42, N, 12.02.

2,2'-(4,4'-(4-Methylphenylazanediyl)bis(4,1-phenylene)bis(methan-1-yl-1-ylidene))dimalononitrile (4) ^{1}H BMR (700 MHz, $CDCl_3$, δ, ppm): 7.26 (d, 4H, *J* = 8.8 Hz, Ar), 7.62 (s, 2H, CH), 7.25 (d, 2H, *J* = 8.2 Hz, Ar), 7.17 (d, 4H, *J* = 8.8 Hz, Ar), 7.06 (d, 2H, *J* = 8.2 Hz, Ar), 2.40 (s, 3H, CH_3). ^{13}C NMR (176 MHz, $CDCl_3$, δ, ppm): 158.8, 138.7, 135.6, 128.8, 124.8, 121.8, 116.8, 114.4, 113.2, 78.1, 26.6. IR (KBr), ν, cm^{-1}: 3028 (C-H_{ar}), 2922 (C-H_{aliph}), 2223 (C≡N), 1567, 1500 (C=C), 1338, 1295 (C-N), 1331, 1303, 1291 (C-$H_{tret.amin.}$), 830 (C-H_{ar}); MS (APCI$^+$, 20 V), m/z: 434 ([M+Na]$^+$); Anal. Calcd for $C_{27}H_{17}N_5$ (%): C, 78.81; H, 4.16; N, 17.02. Found (%): C, 78.86, H, 4.14, N, 17.04.

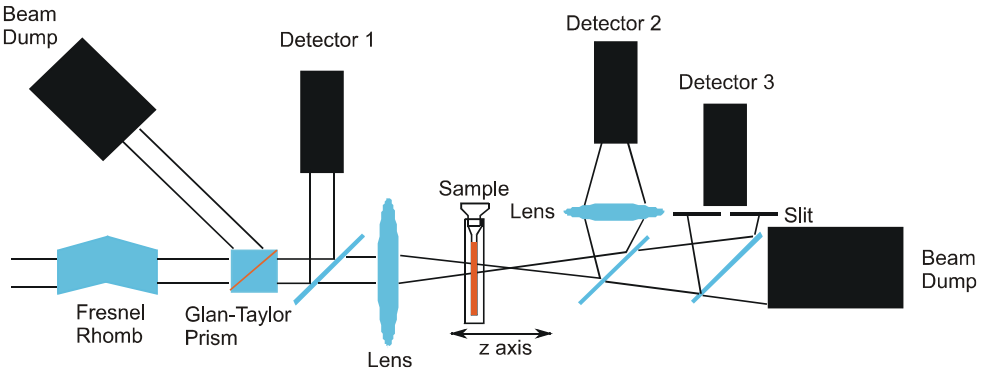

Figure S1. Z-scan experimental set-up. Laser beams power was measured with three detectors. Detector 1 measured reference signal to exclude any external influence on measurements. Detector 2 gave open aperture signal and detector 3 gave closed aperture signal.

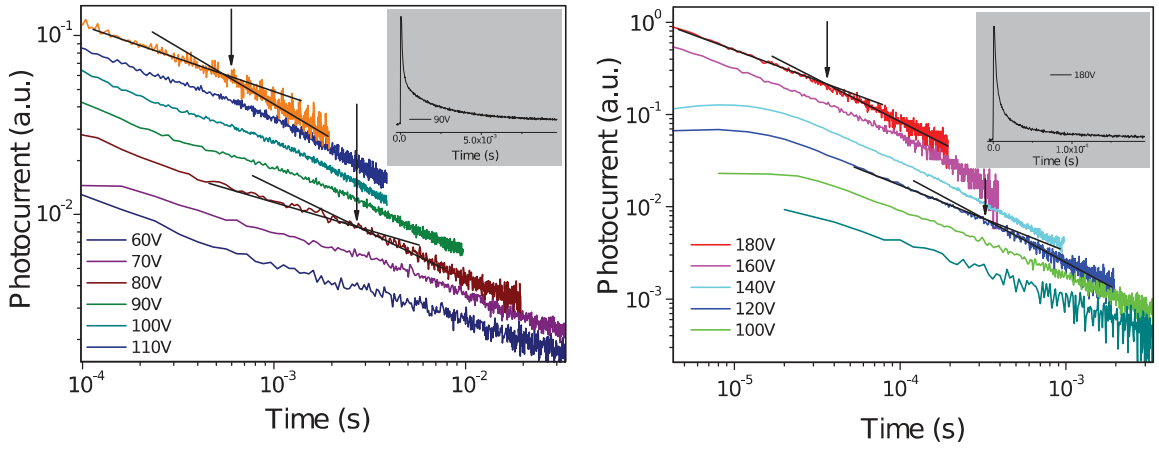

a) b)

Figure S2. Photocurrent transients for holes of compound **1** (a) and for electrons of compound **1** (b) in log-log scales. The arrows indicate t_{tr} for two different electric fields. As an example, a photocurrent transient is showed in linear scales (insert).

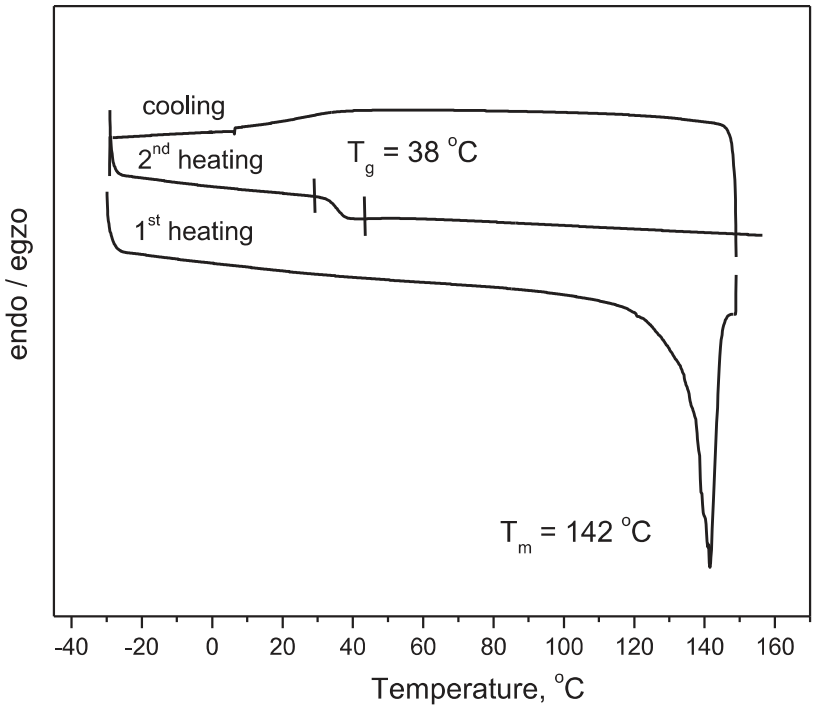

Figure 1. DSC thermograms of compound **1** (scan rate of 10 ºC/min, N_2 atmosphere).

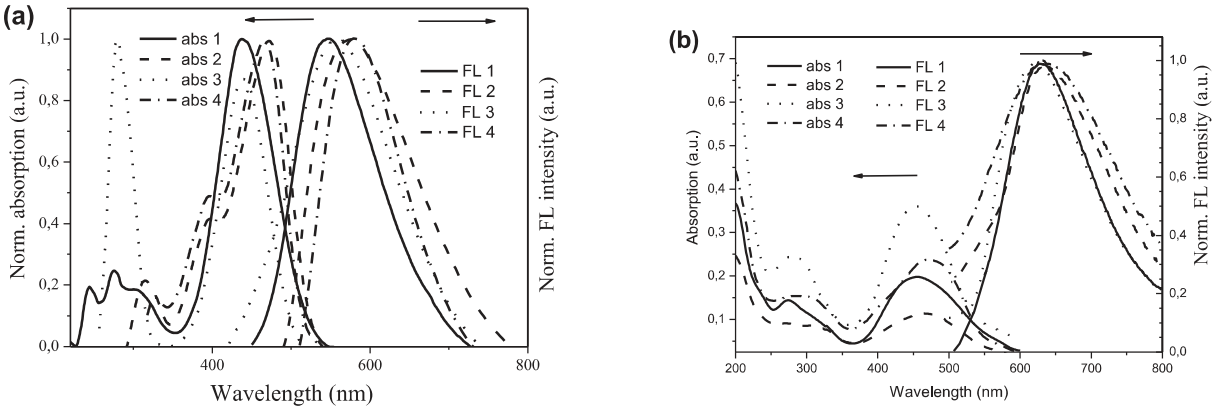

Figure 2. (a) Normalized absorption, FL spectra of dilute solutions of **1-4** in THF (10^{-5} M); (b) absorption and normalized FL spectra of solid films of **1-4**. The wavelengths of low-energy absorption maxima were used as excitation wavelengths.

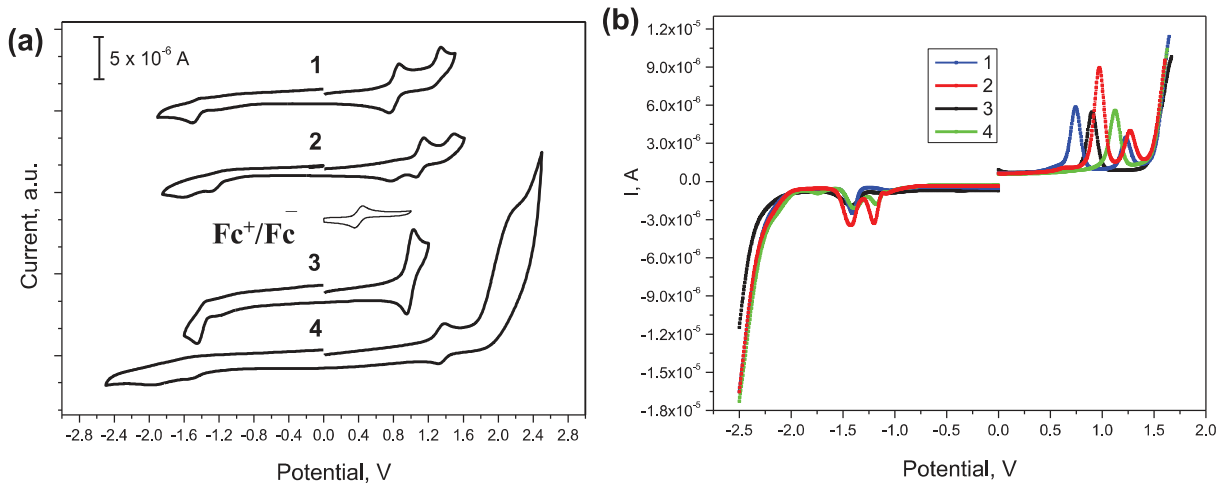

Figure 3. (a) CV of **1-4** (c = 10^{-6} M) recorded in the inert atmosphere. Scan rate 100 mV s^{-1}, electrolyte 0.1 M Bu_4NPF_6 in DCM; (b) DPV curves of 1mM of the solutions of compounds **1-4** in 1M Bu_4NBF_6 in DCM electrolyte.

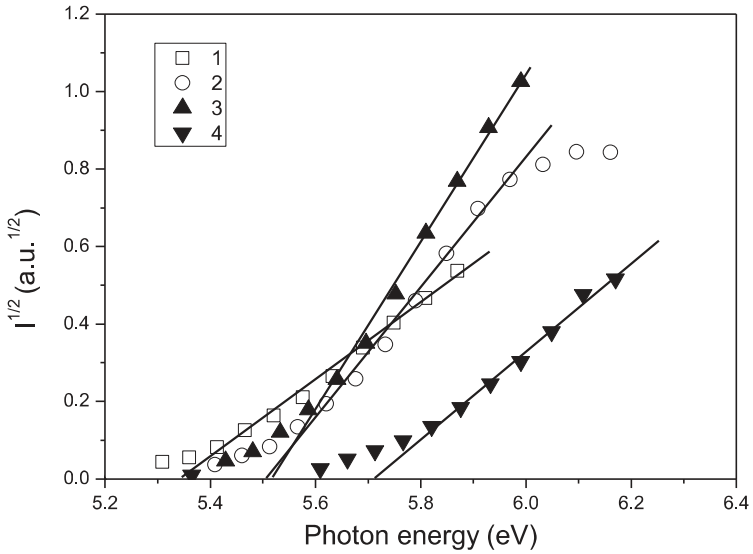

Figure 4. Photoelectron emission spectra of the solid films of compounds **1-4**.

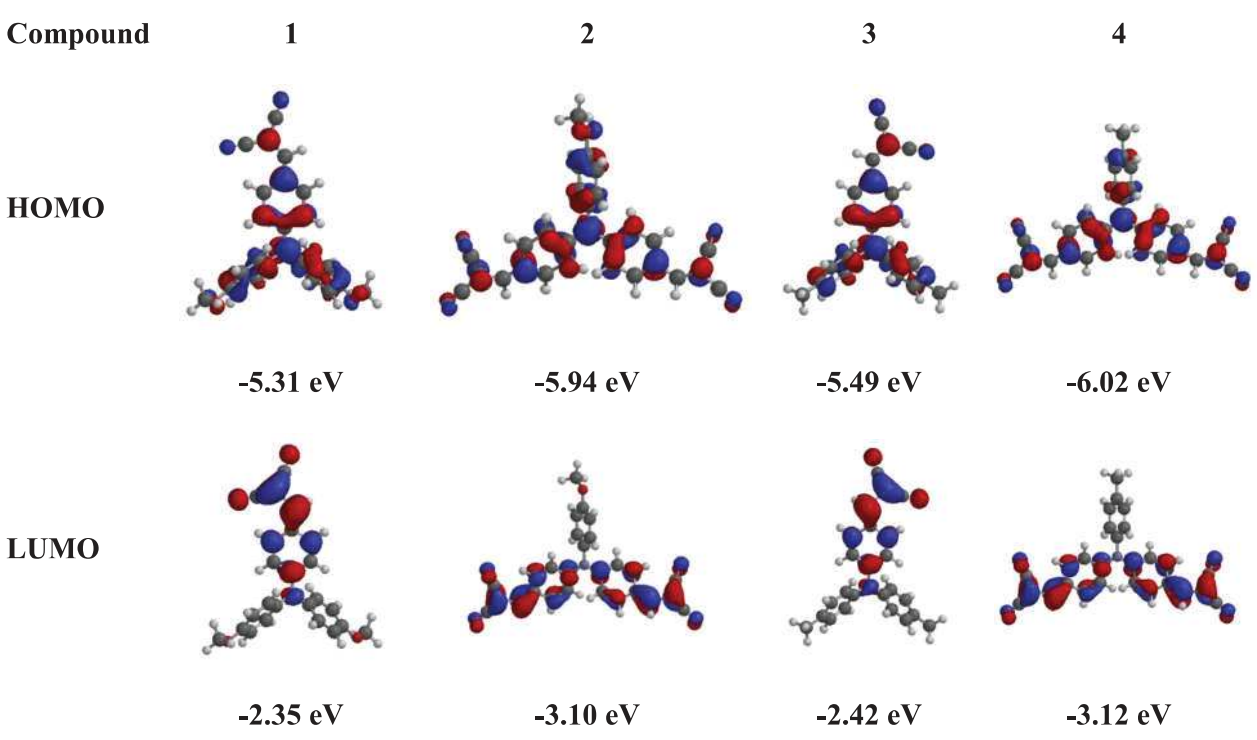

Figure 5. Frontier orbital plots for compounds **1-4**.

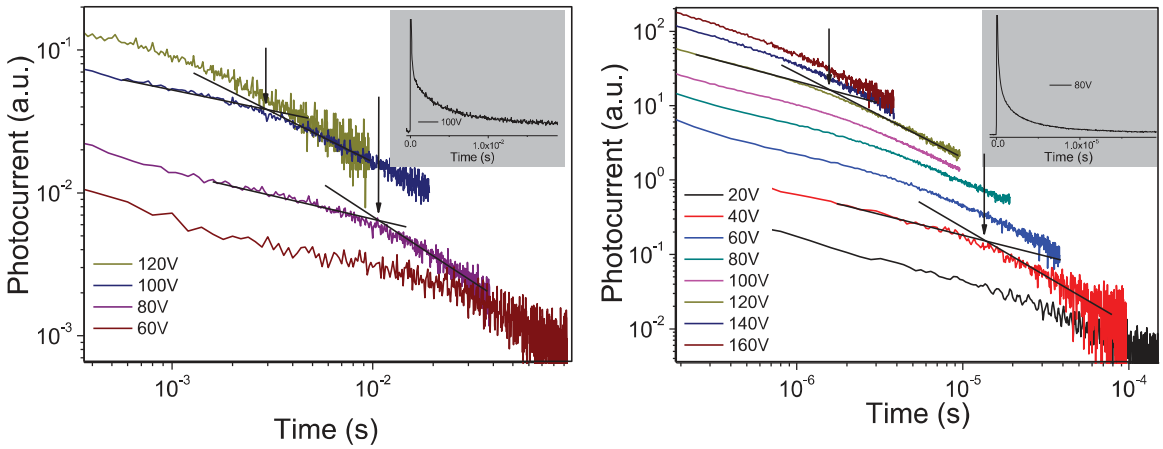

a) b)

Figure 6. Photocurrent transients for holes of compound **2** (a) and for electrons of compound **2** (b) in log-log scales. The arrows indicate t_{tr} for two different electric fields. In the inserts, photocurrent transients in the linear scales are shown.

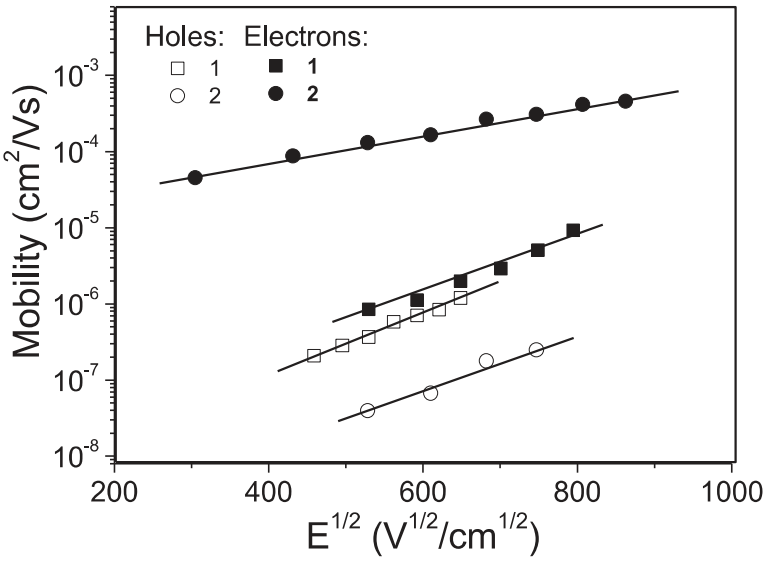

Figure 7. Electric field dependences of hole and electron mobilities of the layers of compounds **1** and **2** recorded at room temperature.

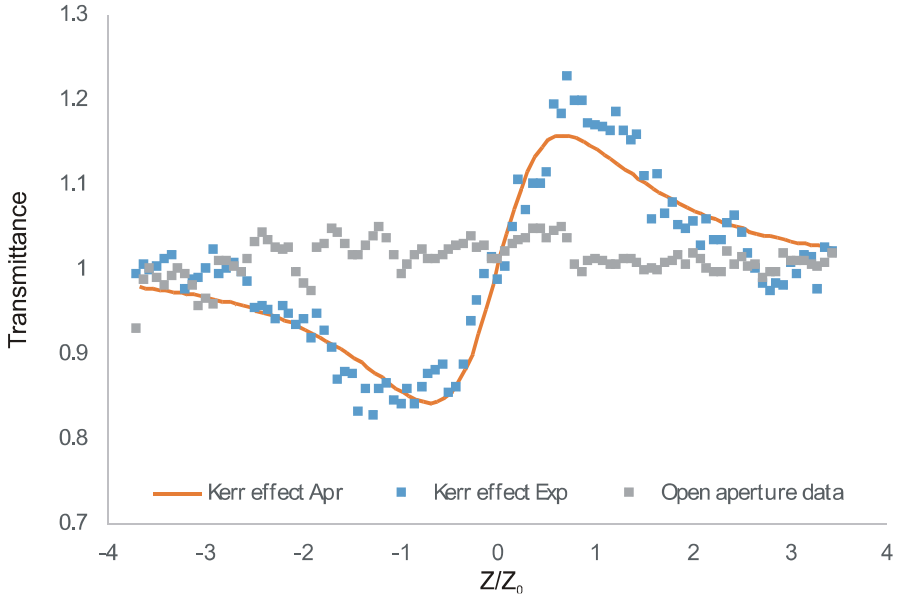

Figure 8. Experimental data. Kerr effect data were acquired by dividing closed aperture data with open aperture data.

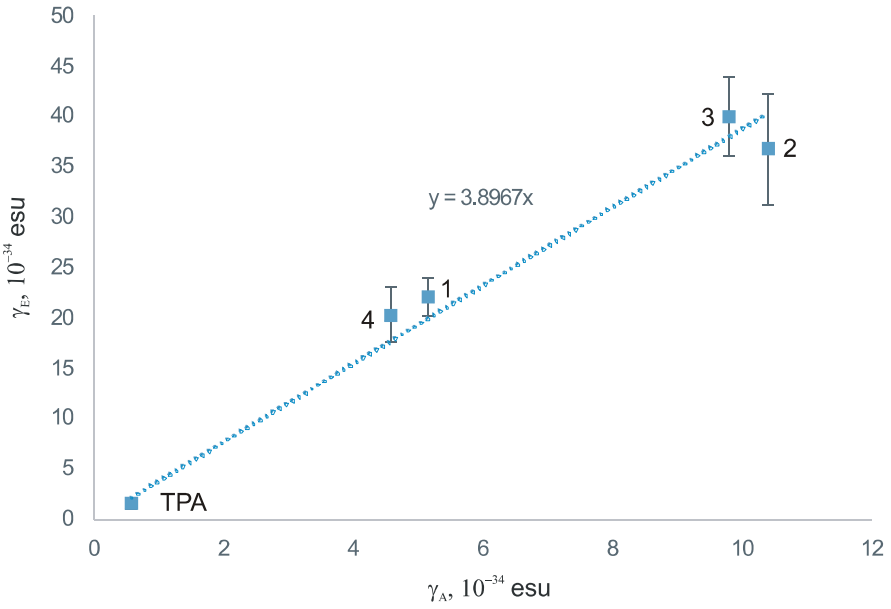

Figure 9. Experimental and theoretical values of second order hyperpolarizability.

Table 1. Thermal characteristics of compounds **1-4**.

Compound	T_m, [^oC][a]	T_g, [°C][b]	$T_{ID-5\%}$, [°C][c]
1	142	38	307
2	152	51	284
3	138	85	323
4	207	107	297

[a] Scan rate 10 °C/min, N_2 atmosphere, T_g - glass-transition temperature, T_m - melting temperature. [b] Second heating scan. [c] Scan rate 20 °C/min, N_2 atmosphere, $T_{ID-5\%}$ - 5% weight loss temperature.

Table 2. Absorption and emission characteristics of the solutions of **1-4** in various solvents and of the solid films.

Compound		Solvent			
		Toluene	Chloroform	THF	Solid film
1	λ_{abs} [a], nm	444	450	437	453
	λ_{em} [b], nm	529	540	547	621
	Φ_F [c], %	35.2	0.7	0.3	1.8
	Stokes shift, nm	85	90	110	168
2	λ_{abs} [a], nm	474	485	472	503
	λ_{em} [b], nm	556	565	580	633
	Φ_F [c], %	33.7	1.9	1.7	2.0
	Stokes shift, nm	82	80	108	130
3	λ_{abs} [a], nm	443	452	438	454
	λ_{em} [b], nm	528	542	558	628
	Φ_F [c], %	42.5	4.9	2.3	8.6
	Stokes shift, nm	85	90	120	174
4	λ_{abs} [a], nm	472	482	468	505
	λ_{em} [b], nm	548	557	573	637
	Φ_F [c], %	38.7	6.8	5.7	9.6
	Stokes shift, nm	76	75	105	132

[a] Peak wavelength of absorption bands. [b] Wavelength at fluorescence band maximum. [c] FL quantum yield.

Table 3. Electrochemical and photoelectrical characteristics of compounds **1-4**.

Compound	$E_{onset}^{ox_1}$ / $E_{onset}^{ox_2}$ *vs* Fc/V	$E_{onset}^{red_1}$ / $E_{onset}^{red_2}$ *vs* Fc/V	IP_{CV} /eV[a]	EA_{CV} /eV[a]	IP_{EP} /eV[b]	E_g^{op} /eV[c]	E_g^{op} /eV[d]	E_g^{el} /eV[e]
1	0.51/0.98	-1.75	5.31	-3.05	5.36	2.38	2.16	2.26
2	0.66/1.13	-1.51/-1.69	5.46	-3.29	5.53	2.35	2.21	2.17
3	0.69/-	-1.69	5.49	-3.11	5.55	2.48	2.23	2.38
4	0.91/-	-1.39/-1.62	5.71	-3.41	5.74	2.40	2.20	2.30

[a] $IP_{CV} = -(E_{onset}^{ox_1}+4.8)$; $EA_{CV} = -(E_{onset}^{red_1}+4.8)$ (where, $E_{onset}^{red_1}$ and $E_{onset}^{ox_1}$ are onset reduction and oxidation potentials *versus* the Fc^+/Fc); [b] IP_{EP} - ionization potentials of thin solid layers; [c] $E_g^{op} = 1240/\lambda_{edge}$, in which the λ_{edge} is the onset value of absorption spectrum of dilute DCM solution in long wave direction; [d] E_g^{op} for solid film; [e] $E_g^{el} = IP_{CV} - EA_{CV}$.

Table 4. Experimental values of nonlinear refractive index n_2, the real part of third-order susceptibility χ_{Re} and second-order hyperpolarizability γ_E, as well as the results of quantum chemistry calculations of second order hyperpolarizability γ_A.

Compound	n_2, cm^2/W	χ_{Re}, esu	γ_E, esu	γ_A, esu
TPA	$(8.6\pm2.9)\cdot10^{-14}$	$(4.5\pm1.5)\cdot10^{-12}$	$(16.9\pm5.7)\cdot10^{-35}$	$5.8\cdot10^{-35}$
1	$(111.9\pm9.5)\cdot10^{-15}$	$(13.7\pm1.2)\cdot10^{-12}$	$(22.1\pm1.9)\cdot10^{-34}$	$5.20\cdot10^{-34}$
2	$(19.7\pm3.0)\cdot10^{-14}$	$(24.2\pm3.6)\cdot10^{-12}$	$(36.7\pm5.5)\cdot10^{-34}$	$10.4\cdot10^{-34}$
3	$(21.3\pm2.1)\cdot10^{-14}$	$(26.1\pm2.5)\cdot10^{-12}$	$(40.0\pm3.9)\cdot10^{-34}$	$9.80\cdot10^{-34}$
4	$(13.4\pm1.8)\cdot10^{-14}$	$(16.5\pm2.2)\cdot10^{-12}$	$(20.3\pm2.7)\cdot10^{-34}$	$4.60\cdot10^{-34}$

Donor and acceptor substituted triphenylamines exhibiting bipolar charge-transporting and NLO properties

Dalius Gudeika, Arturs Bundulis, Igors Mihailovs, Dmytro Volyniuk, Juozas V. Grazulevicius, Martins Rutkis

Highlights

- Derivatives of triphenylamine based malonodinitriles were synthesized.
- Their glass transition temperatures range from 38 to 107 ^{o}C.
- Electron mobility values reached 4.56×10^{-4} cm^2/V·s at electric field of 7.5×10^5 V/cm.
- All the molecules had positive sign for second order hyperpolarizability.